Article

Ferrocenylimine Palladium (II) Complexes: Synthesis, Characterization and Application in Mizoroki-Heck and Suzuki-Miyaura Cross-Coupling Reactions

Asanda C. Matsheku [1], Richard Tia [2], Munaka C. Maumela [1] and Banothile C. E. Makhubela [1,*]

[1] Centre of Synthesis and Catalysis, Department of Chemical Sciences, University of Johannesburg, P.O. Box 524, Auckland Park, Johannesburg 2006, South Africa; mtsasa002@myuct.ac.za (A.C.M.); cmaumela@uj.ac.za (M.C.M.)

[2] Department of Chemistry, Kwame Nkrumah University of Science and Technology, Kumasi 1916, Ghana; richardtia.cos@knust.edu.gh

* Correspondence: bmakhubela@uj.ac.za; Tel.: +27-11-559-3782

Abstract: Carbon-carbon cross-coupling reactions are essential synthetic tools for synthesizing polymers, natural products, agrochemicals, and pharmaceuticals. Therefore, new catalysts that function with greater efficiency and functional group tolerance are being researched. We have prepared new ferrocenylimine monodentate N and P donor ligands and NˆN and NˆP bidentate chelating ligands (**L1** to **L4**) employed in stabilizing palladium ions for application in Mizoroki-Heck and Suzuki-Miyaura cross-coupling reactions. The ferrocenylimine ligands were successfully synthesized by Schiff base condensation reactions of acetyl ferrocene with hydrazine monohydrate to afford ferrocenyl hydrazone (**L1**). Ligand **L1** was further treated with aldehydes to give ferrocenyl(2-diphenylphosphino)imine (**L3**) and ferrocenyl(pyridyl)imine (**L3**), while phosphination of **L1** with chlorodiphenylphosphine afforded **L2**. The ligands were used to prepare new palladium(II) complexes (**C1** to **C4**) by complexation with [PdCl$_2$(MeCN)$_2$]. All the ligands and complexes were fully characterized using standard spectroscopic and analytical techniques, including ^{1}H NMR and ^{13}C NMR spectroscopy, FT-IR spectroscopy, mass spectrometry and elemental analysis. The complexes (**C1** to **C4**) were tested for efficacies in catalyzing Mizoroki-Heck and Suzuki-Miyaura C-C cross-coupling reactions and proved to be suitable catalyst precursors. Ferrocenyl(2-diphenylphosphine)imino and ferrocenyl-methyl hydrazone palladium(II) complexes **C2** and **C3** showed the best activities at TONs of up to 201. The ferrocenyl palladium(II) (pre)catalysts demonstrated moderate activity in Mizoroki-Heck reactions involving substrates with substituents on the olefin and aryl halide (including 4-Cl, 4-CH$_3$, -CO$_2$Me and -CO$_2$Et). Density Functional Theory was used to study the mechanism of the Mizoroki-Heck cross-coupling reactions and have led to confirmation of the widely accepted catalytic cycle. Catalyst precursors (**C1** to **C4**) also displayed good activity and selectivity in Suzuki-Miyaura cross-coupling reactions, at 0.5 mol% catalyst loading, with good tolerance to functional groups present on the aryl halide and boronic acid substrates (such as 4-Cl, 4-CHO, 4-COOH, 3-NO$_2$, 3,5-dimethoxy and 4-CH$_3$).

Keywords: palladium(II) complexes; Mizoroki-Heck; Suzuki-Miyaura; cross-coupling; ferrocenyl ligands; electrochemistry

1. Introduction

Carbon-carbon (C-C) cross-coupling reactions are used to assemble or couple two different hydrocarbon fragments in the presence of metal catalysts. These reactions result in the formation of new C-C bonds, specifically bonds between combinations of sp^2 carbon atoms [1], that are essential for constructing pharmaceutical, agrochemical and various fine chemical products [2]. Successful cross-coupling approaches were achieved using palladium and nickel, with reports suggesting that nickel is inferior to palladium [3]. Nickel

is limited by lack of functional group tolerance and competitive halogen-metal exchange during reactions leading to homocoupling products [4]. Palladium is a noble precious-metal, which is more stable than non-precious metals such as nickel and its utilization has gained extensive attention. The demand is further motivated by palladium's abundant availability [5].

Aryl bromides, iodides and triflates are easily activated by palladium catalysts and are often employed for the Mizoroki-Heck and Suzuki-Miyaura cross-coupling reactions. The more economical but less reactive aryl chlorides do not react except when they are activated by electron-withdrawing groups in Suzuki-Miyaura cross-coupling reactions with boronic acids [6], whereas in Mizoroki-Heck cross-coupling reactions, the coupling of aryl chloride with olefins remains challenging [7]. These challenges have been tackled by designing bulky and electron-rich ligands, such as dialkylphosphine, dialkylbiarylphosphines, and ferrocenyl-based ligands, etc., [8–10], which have allowed or facile cross-coupling of aryl halides (including aryl chlorides) with boronic acids and olefins, respectively [8,11–16].

Ligand design, including its steric and electronic properties, significantly influences the outcome of the most crucial steps in cross-coupling reactions namely; oxidative addition and reductive elimination [14]. Recent advances have explored the use of ferrocenyl-based ligands in palladium-catalyzed cross-coupling reactions [17], due to 'ferrocene's unique properties. Ferrocene possesses favourable electronic properties, is synthetically flexible and stable at high temperatures. It is also tolerant to water, alkali and acidic conditions, making it an ideal candidate for inclusion in ligands to be used in catalysis. In cross-coupling reactions, the ferrocene moiety can further add to the 'catalyst's bulk, promoting reductive elimination in the catalytic cycle [17].

Ferrocenyl ligands have been investigated and were found to generate more active catalysts for cross-coupling reactions [15]. This is because, with ferrocenyl supporting ligands, the active metal can demonstrate redox-switchable catalysis (RSC) properties, where its oxidized form displays a higher catalytic rate than the non-oxidized version of the same catalyst [18]. The most commonly used ferrocenyl ligand is 1,1-*bis*(diphenylphosphino) ferrocene, dppf, which is best known for its wide range of unique applications [17]. Dppf was first discovered and used in 1965 [19], and its applications have grown to include C-C cross-coupling reactions (Mizoroki-Heck, Suzuki-Miyaura) [17,20].

The application of dppf in Suzuki-Miyaura cross-coupling of less reactive and less costly substrates (such as chloroarenes) proved to be difficult [20]; however, there are numerous examples of successful Suzuki-Miyaura cross-coupling of aryl and heteroaryl iodides, triflates and bromides with boronic acids using PdL$_2$ and **1.1** [21–24] type ligands (L = Cl or OAc). Only a few reports exist on Mizoroki-Heck coupling reactions, where dppf and other ferrocenyl phosphines are used. Therefore, there is an opportunity to develop other ferrocenyl derivatives for this purpose [25,26]. In one of the few examples, Hii and co-workers reported the coupling of methyl methacrylate with 4-bromoacetophenone by [Pd(OAc)$_2$(dppf)] (0.01 mol%) at 140 °C in DMF (96% yield, TON 9600) [27].

The air-stable and sterically hindered ferrocenyl ligand (**1.2**) has been reported to have successfully catalyzed C-O, C-N and C-C (Suzuki-Miyaura) cross-coupling reactions and good yields were obtained (78–98%) [28] (Figure 1). Hartwig and co-workers reported that **1.2** combined with [Pd(dba)$_2$] catalyzed Mizoroki-Heck coupling of activated and deactivated aryl bromides with methyl methacrylate. Yields of up to 95% were recorded at room temperature using DMF solvent and **1.2** equivalents of Et$_3$N [29].
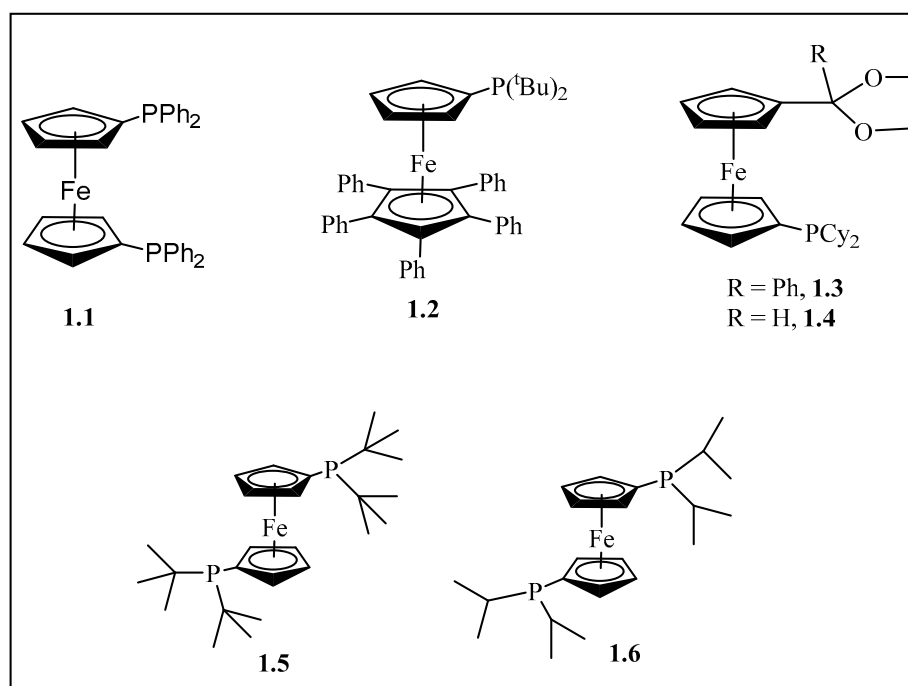
Figure 1. The structure of the bidentate ligand 1,1-*bis*(diphenylphosphino) ferrocene, dppf, (**1.1**) [20]. Sterically demanding ferrocenyl ligand (**1.2**) [15] and P^O-functionalized ferrocenyl ligands (**1.3**) and (**1.4**) [30]. 1,1′-*Bis*(di-tertiarybutyl phosphino)ferrocene (**1.5**) and 1,1′-*bis*(di-isopropyl phosphino)ferrocene (**1.6**) ligands [31,32].

Suzuki cross-coupling of aryl chlorides with substituted and unsubstituted phenylboronic acid was reported by Teo et al. [30]. In these studies, the authors noted that 0.2 mol% [Pd(dba)$_3$] and **1.3** or **1.4** gave yields as high as 100% in 16 h [30].

In addition, aryl and heteroaryl chlorides were coupled with phenylboronic acid in the presence of [Pd(OAc)$_2$] and **1.5** or **1.6** (Figure 1). These reactions were carried out in 1,4-dioxane using 10 mol% of the catalyst at 80 °C to give 72–92% yields [31,32].

Despite improvements in the activity and selectivity when using bulky phosphine ligands, a significant challenge remains to develop ligand or ligated palladium catalysts that can catalyze broad spectrum cross-coupling reactions using challenging substrates (such as aryl chlorides). Ferrocenyl moieties can produce ligands that are electron-rich and bulky. Furthermore, the use of Schiff base chemistry to deliver ferrocenylimine-based scaffolds presents an opportunity to develop air- and moisture-stable ligands. As such, we aimed to contribute to this field by synthesizing ferrocenylimine ligands as new entries to the bulky and electron-rich ligand family. These ligands were then used in palladium-catalyzed Mizoroki-Heck and Suzuki-Miyaura cross-coupling reactions.

2. Results and Discussion

2.1. Synthesis and Characterization of Ligands, **L1**–**L4**

The synthesis of **L1**–**L4** was achieved via Schiff base condensation reactions as outlined in Scheme 1, where **L1** was prepared following a modified literature protocol reported by Shu-Sheng and co-workers [33–35]. These ligands were isolated in moderate to good yields and revealed excelled solubility in organic and chlorinated solvents such as DCM, MeCN, DMSO, THF, toluene and DMF. Ferrocenyl hydrazone (**L1**) is a known compound, all the expected ^{1}H-NMR peaks were observed, and they agree with those reported by Shu-Sheng and co-workers [33], with the N*H*$_2$ proton signal appearing upfield at 5.83 ppm (Figure S1, supplementary materials).
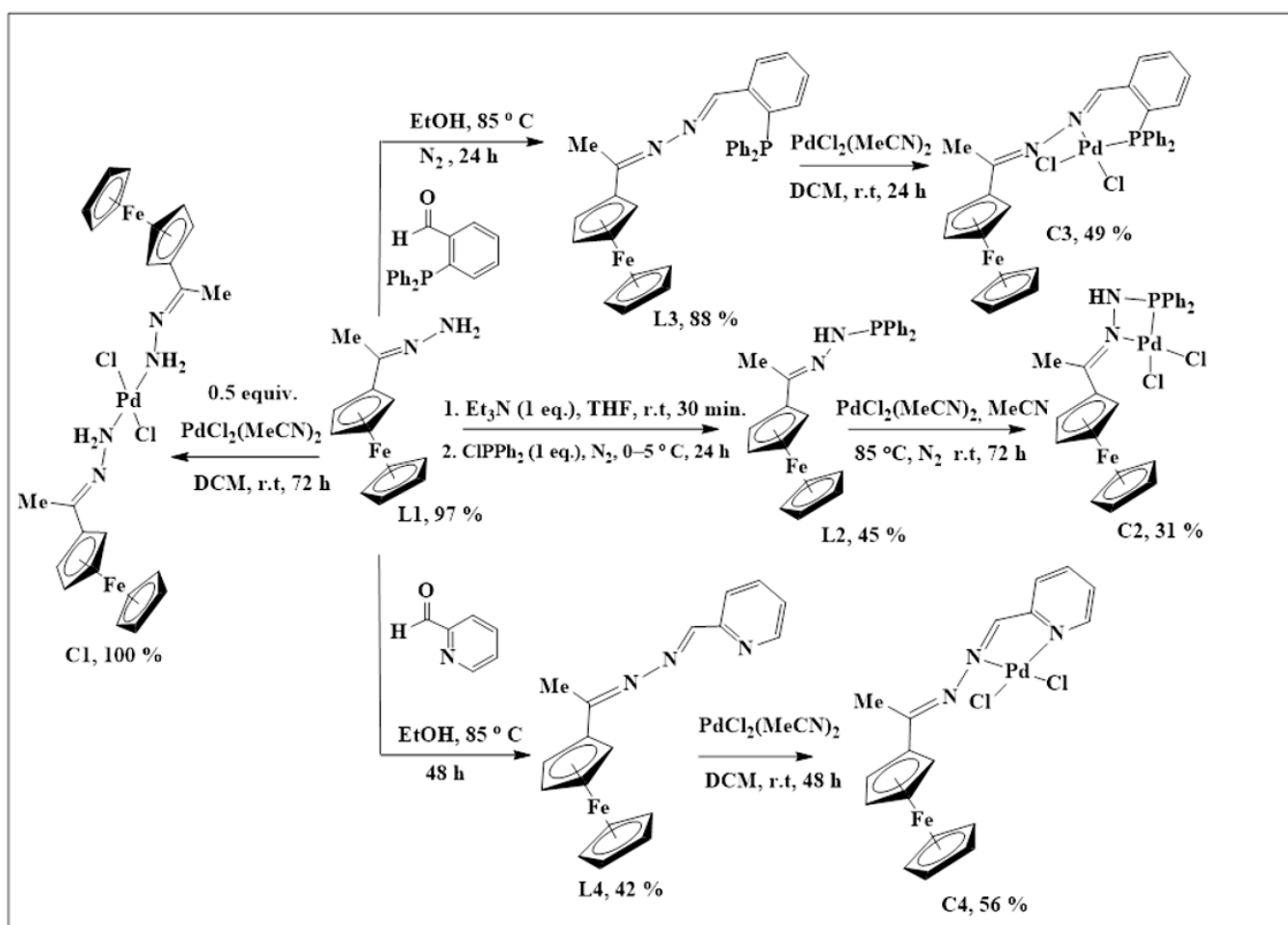
Scheme 1. The synthesis of ferrocenyl-imine ligands **L1–L4** and their Pd(II) complexes.

The successful nucleophilic substitution (S$_N$2) of **L1** to **L2** was confirmed by the proton NMR disappearance of the NH_2 proton signal with the appearance of aromatic peaks, assigned to the—P*Ph*$_2$ moiety (7.36–7.57 ppm), was a strong indication that the desired ligand (**L2**) was synthesized. The ^{31}P{^{1}H}-NMR revealed one signal at 23.6 ppm as expected, therefore providing further support that **L2** has been successfully isolated (Figure S2).

Once again, the disappearance of the NH_2 peak at around 5.80 ppm (in **L1**) was observed in the proton NMRs of **L3** and **L4**. The proton NMR spectrum of **L3** showed a broad signal at 8.71 ppm, assigned to H$_k$, the imine proton (Figure S3). The phosphorus atom is shielded due to the delocalization of electrons towards this atom, caused by the aromatic rings it is attached to. Therefore, the phosphorus NMR spectrum of **L3** displayed a signal in the negative region at −13.1 ppm (Figure S4) [36]. The carbon NMR also suggested that L4 was isolated successfully by revealing all the expected characteristic carbon signals (Figure 2) where the methyl (*Me*) carbon signal was seen upfield at 15.3 ppm (**C$_h$**). The two signals are seen at 167.1 ppm and 152.8 ppm are of approximately equal intensity and were assigned to the imine carbons (C=N), C$_g$, and C$_e$. The imine carbon (C=N), C$_f$, gave rise to the signal at 155.6 ppm.
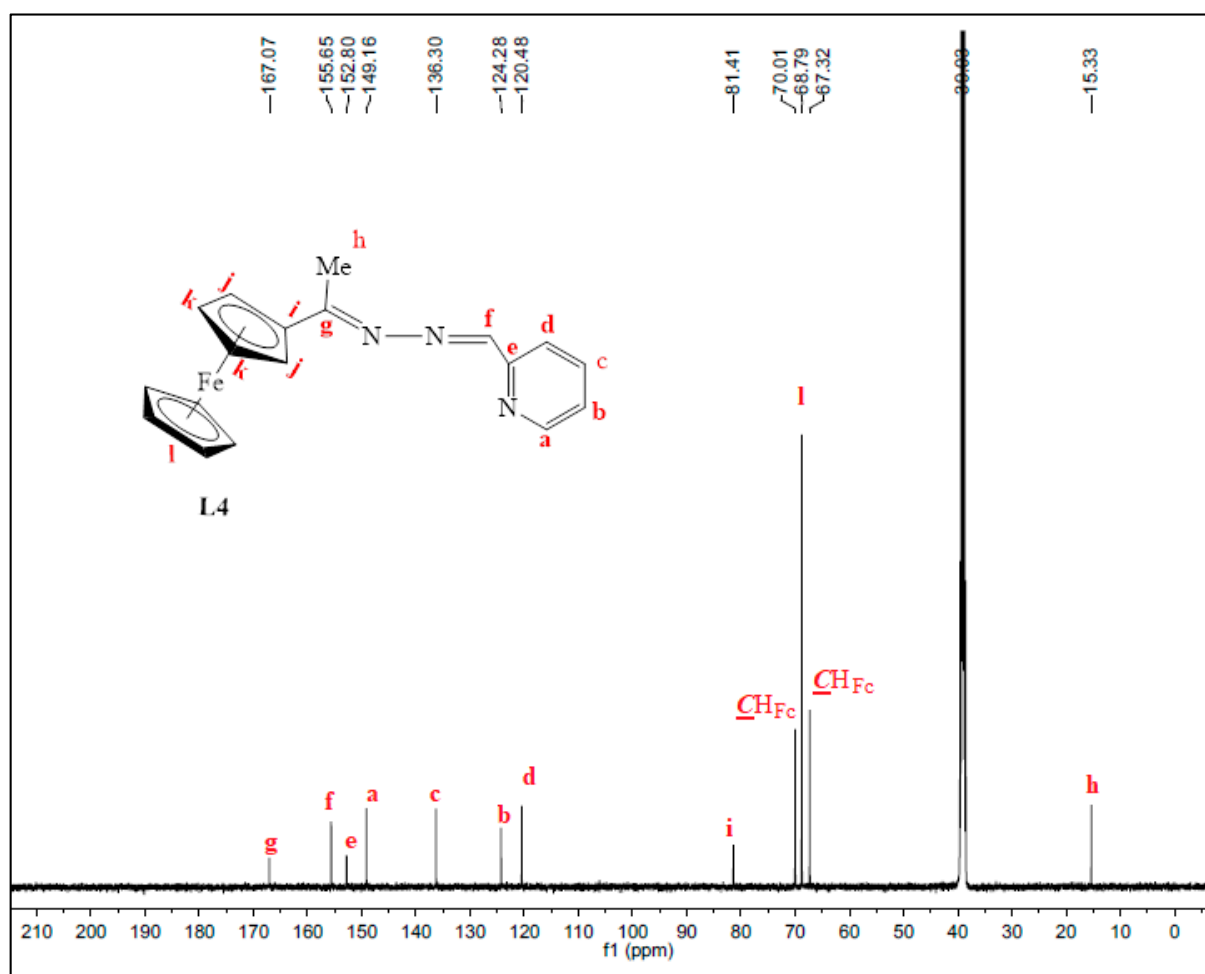
Figure 2. ^{31}C-NMR spectrum of **L4**, recorded in DMSO-d_6 at 25 °C.

2.2. Synthesis and Characterization of Complexes, **C1–C4**

The synthesis of complexes **C1–C4** has been summarized in Scheme 1. All the complexes (**C1–C4**) had poor solubility in solvents such as THF, DCM, diethyl ether, ethanol and acetone, but were soluble in DMSO, DMF and acetonitrile. Upon coordination to the palladium centre, the proton NMR signals, in **C1–C4**, showed explicit shifts (or disappearance) of proton resonances compared to the same signals in the free ligands (**L1–L3**). This was the first suggestion that the complexation of the palladium to the ligands was successful.

For example, in the ^{1}H-NMR spectrum of **L1** (Figure S1), the NH_2 protons were seen at 5.83 ppm, and upon complexation, this peak shifted downfield to 7.46 ppm (Figure S6). The proton NMR spectrum of **C1** (Figure S6) also showed the ferrocenyl protons CH$_{Fc}$ (4.38 ppm and 4.43 ppm) and CH$_{Fc}$ (4.61 ppm and 4.66 ppm), which appear to split, suggesting the presence of *cis* and *trans* isomers of **C1** (Figure 3) It is likely that the major isomer is the *trans* since steric crowding would make the isomer less stable in solution [37–40]. However, **C1** is very insoluble and is soluble in DMSO only, which restricted the attempt to separate the isomers by recrystallization. Furthermore, when **C1** was kept in the DMSO solution for over four hours at room temperature, the solution changed colour from purple to black, suggesting decomposition.
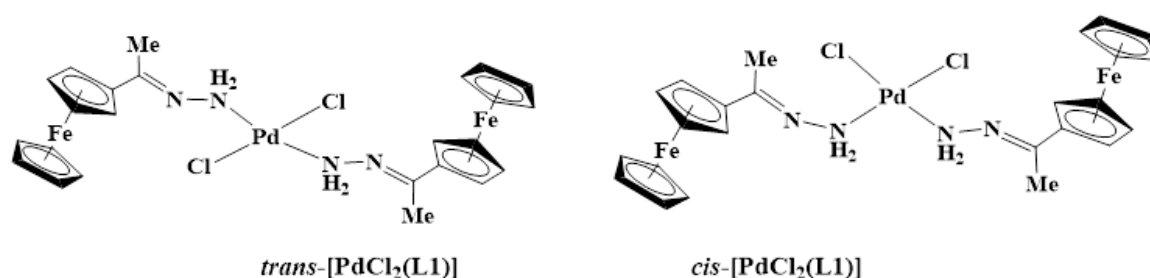
Figure 3. Structures of *cis*- and *trans*-dichlorobis(ferrocenyliminehydrazone)palladium(II) complex **C1**.

The ^{31}P{^{1}H}-NMR spectrum of **C2** gave further evidence that the palladium centre was coordinated to the phosphine successfully to form one species since this spectrum only displayed one peak at 105.6 ppm (Figure S7). This signal has shifted downfield from 23.6 ppm (in **L2**, Figure S2), indicating that the palladium centre pulls the electrons towards itself upon complexation, thus resulting in de-shielding of the phosphorus atom. In complex **C2**, (C=N)$_{imine(Me)}$ stretching frequency band experience a more pronounced shift (from 1596 cm^{-1} in **L2** to 1563 cm^{-1} in **C2**) therefore indicating that coordination had taken place at the (C=N)$_{imine(Me)}$ nitrogen as well. Thus, **L2** coordinated to palladium in a bidentate, N^P, fashion forming a strained 4-membered ring palladacycle (**C2**). Upon coordination to palladium, the proton NMR spectrum of **C3** revealed a shift in the signal assigned to the imine (-N=CH) proton H$_k$ from 8.78 ppm (in **L3**, Figure S3) to 8.29 ppm in **C3** (Figure 4). The correlation of the carbon signals with the proton signals (2D NMR, HSQC) was further used to confirm this, which assisted in the assignment of the aromatic carbon signals –CH*Ar*P*Ph*$_2$ (Figure S9). Furthermore, **C3** was confirmed by mass spectrum which revealed the m/z = 654.0021 [M–Cl]$^+$ (Figure S8).

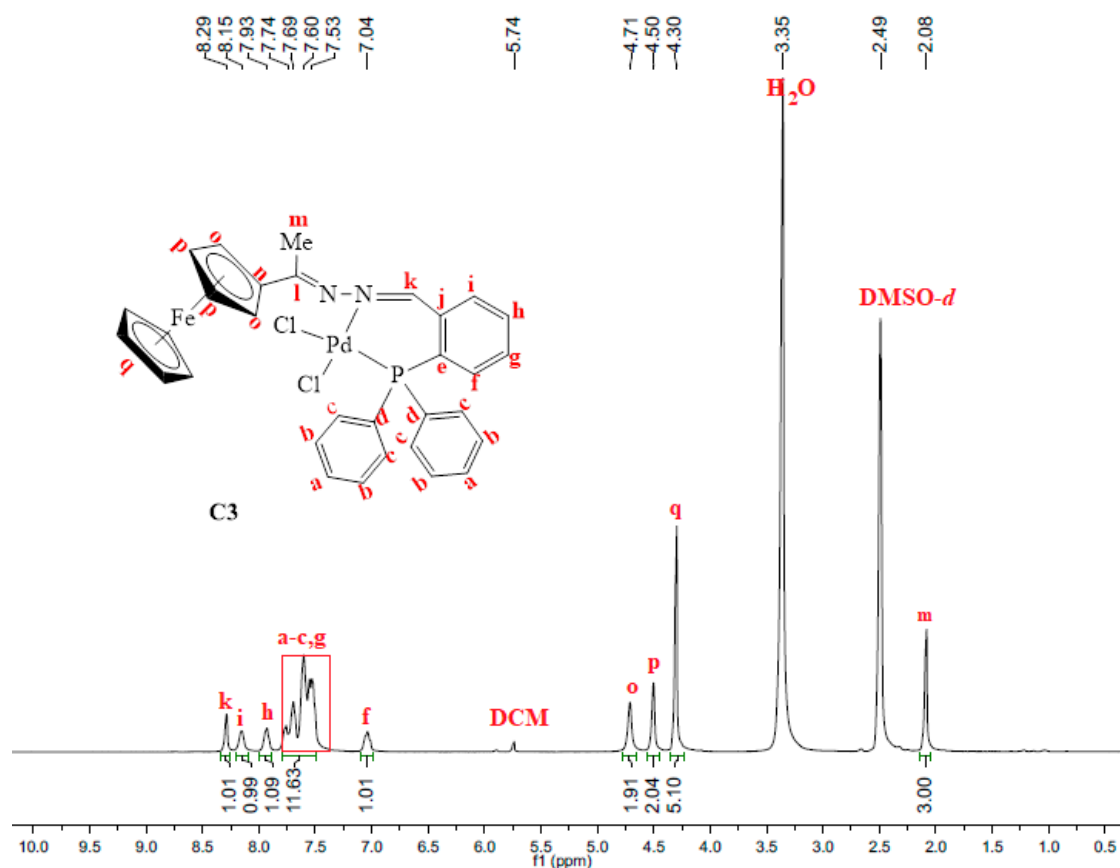**Figure 4.** ^{1}H-NMR spectrum of **C3**, recorded in DMSO-d_6 at 25 °C.

In the ^{1}H-NMR spectrum of **C4**, a shift in the proton NMR signals due to the proton adjacent to the pyridyl nitrogen (H$_a$) and the imine (H$_k$, N=CH), from 8.20 ppm and 8.65 ppm to 8.33 ppm (Figure S5) and 8.92 ppm respectively, confirmed coordination to the palladium in a bidentate fashion. In general, the infrared spectra of complexes **C3** and **C4** showed the (C=N)$_{imine}$ stretching frequency band at higher wavenumbers when compared to the ligands. In contrast, the absorption bands assigned to the (C=N)$_{pyridyl}$ stretching frequencies experience shifts to lower wavenumbers of $\approx$1557 cm^{-1} (**C4**) from $\approx$1588 cm^{-1} in **L4**. The former results from the pyridylimine functional groups and the coordinated palladium withdrawing electrons from the (C=N)$_{HAr}$ bond, thereby causing a shift [41].

2.3. Electrochemical Studies

Electrochemical studies were conducted using cyclic voltammetry which measures the current that develops as a function of voltage through a circuit [42,43]. This gives information (if a species is reduced and/or oxidized) about the redox activity of a compound based on the presence of a metal centre and the nature of the functional groups involved on the ligand [44–46]. The presence of ligands with both σ-donor and π-acceptor character (e.g., N^N, N^P ligands) may contribute towards the stability of a compound [47]. Ferrocene forms one of the major motifs which are redox active, and ferrocenyl cyclic voltammograms of such ferrocene-containing compounds have been reported in literature. Therefore, ferrocene has been widely used as a reference of cyclic voltammetry studies and this was the case for this study [48,49].

Most reports on cyclic voltammetry involving metals other than iron in ferrocene focus on ruthenium (in bimetallic complexes) as it also has a better understood cyclic voltammetric pattern [49–51]. Other redox-active centres include osmium, platinum and cobalt for multinuclear compounds [52,53]. We investigated the electrochemical properties of ferrocenylimine palladium(II) complexes (**C1**, **C2** and **C4**). There are a few reports on redox active centres involving palladium(II) complexes and therefore this study will extend this area. [45,46,53–55]

Cyclic Voltammetry Results of **L1** and **L2** with **C1**, **C2** and **C4**

The cyclic voltammograms of **L1** and **C1** are shown in Figure 5 and also include that of the reference ferrocene (**Fc**) for comparison. The voltammogram of **L1** reveals a reversible anodic peak at E$_{pa}$ = 0.24 V (**D**) followed by a corresponding cathodic peak at E$_{pc}$= 0.26 V (**E**) and another irreversible anodic peak at E$_{pa}$ = 0.41 V (**C**) (Table 1, Figure 5). The reversible redox peaks **D** and **E** are assigned to the redox activity of the ferrocenyl metal centre creating one reversible wave at E$_{1/2}$ = 0.25 V and **C** is possibly due to the irreversible oxidation of the imine nitrogen (C=N).
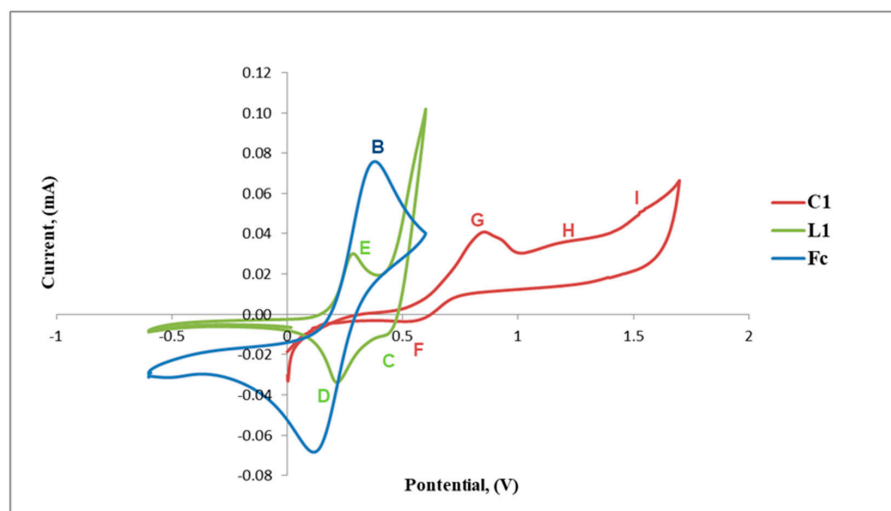

Figure 5. Cyclic voltammograms of ferrocene (**Fc**), **L1** and **C1**.

Table 1. Cyclic voltammetric potentials (V, vs. Ag/Ag$^+$) of **L1**, **C1** and ferrocene (**Fc**).

Compound	Anodic Potentials E_{pa} (V)		Cathodic Potentials, E_{pc} (V)		
Fc	0.14		0.39		
L1	0.24	0.41	0.26		
C1	0.56		0.81	1.17	1.51

(Voltammetric scan range -0.00 to $+1.60$ V). For **Fc** $\Delta E_p = E_{pa} - E_{pc} = -0.25$ V. For **Fc** $E_{1/2} = (E_{pa} + E_{pc})/2 = 0.26$ V.

Upon complexation of **L1** with palladium, the voltammogram of **C1** exhibits a shift of the redox peaks to more positive voltage, where the reversible anodic peak is now observed at $E_{pa} = 0.56$ V (**F**) and the cathodic peak at $E_{pc} = 0.81$ V (**G**) followed by two new broad irreversible cathodic peaks at $E_{pc} = 1.17$ V (**H**) and $E_{pc} = 1.51$ V (**I**). F and G are assigned to the reversible Fe activity forming a wave at $E_{1/2} = 0.68$ V, which is greater than that observed for **L1** ($E_{1/2} = 0.25$ V). The results suggest that the *bis*(ferrocenylimine-hydrazonepalladium(II)complex **C1**, has a ferrocenyl moiety which is more stable than that of the ligand, **L1**, as the redox activity requires increased voltage (Figure 5). The two new broad cathodic peaks could be due to the irreversible reduction of the imine nitrogen (C=N) (**H**) followed by the irreversible putative reduction of palladium(II) to palladium(I) (**I**). We used the voltammogram of palladium(II) acetate to confirm if reduction of palladium(II) to palladium (I) occurred at approximately $E_{pc} = 1.50$ V (≈ 1.51 V, **I**) and this confirmed our hypothesis.

The positive and negative voltammetric scans of **L2** and **C2** are shown in Figure 6. The voltammogram of **L2** exhibits a reversible anodic peak at $E_{pa} = 0.39$ V (**A**) followed by the cathodic peak at $E_{pc} = 0.49$ V (**B**), $E_{1/2} = 0.44$ V, which corresponds to one full wave of ferrocene (Table 2 and Figure 6).
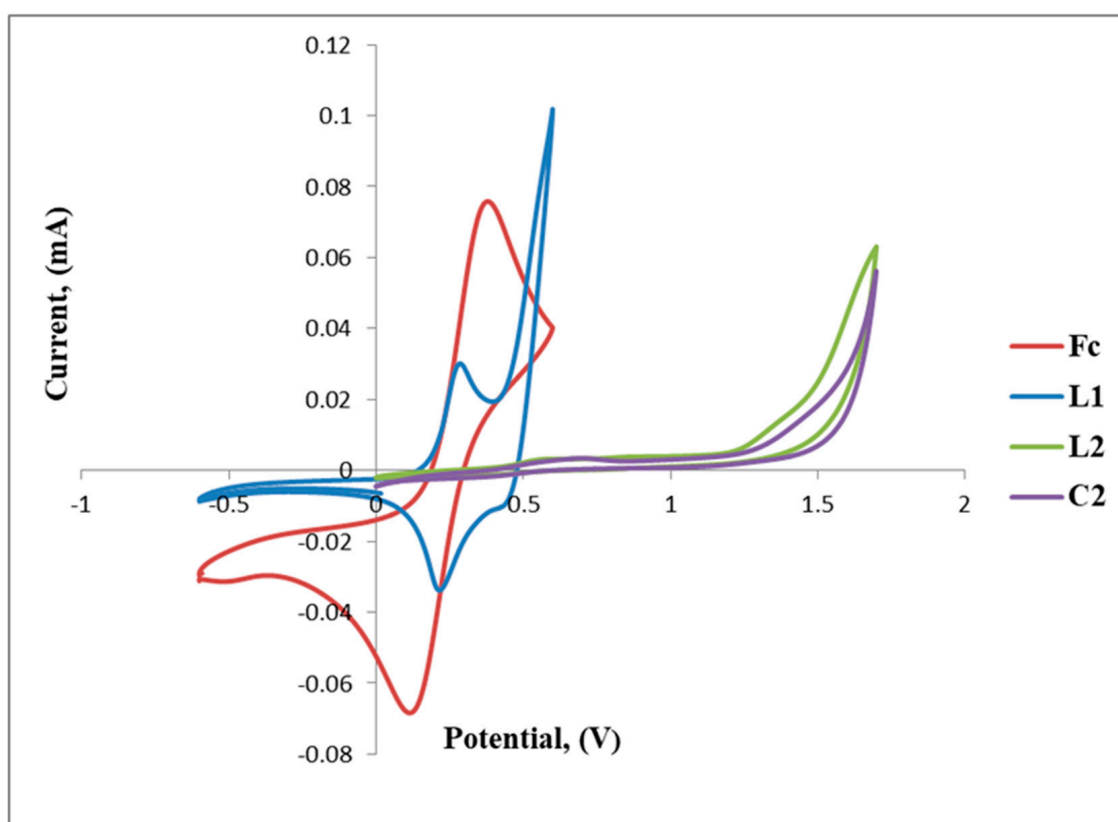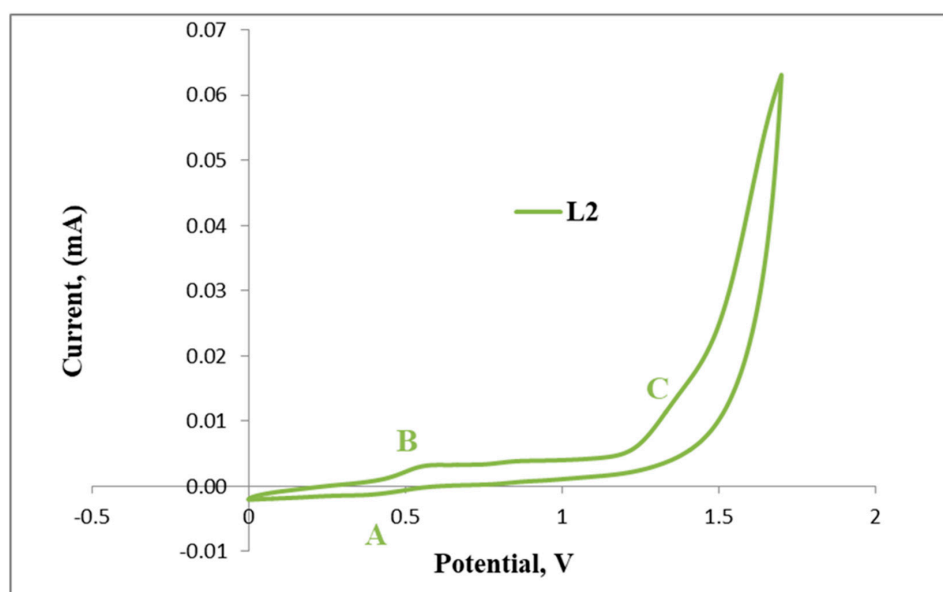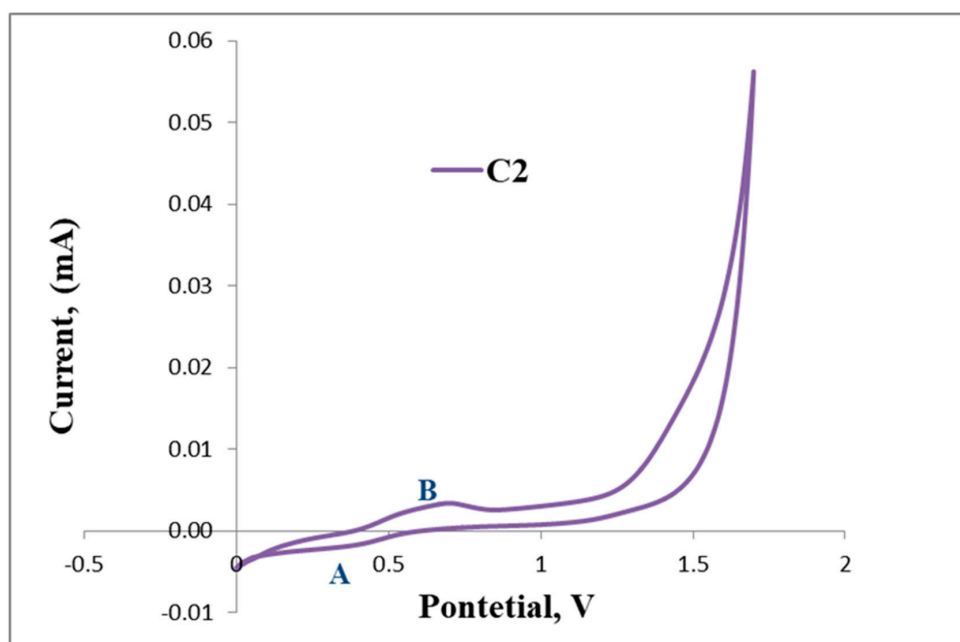

Figure 6. Cyclic voltammograms of ferrocene (**Fc**), **L1**, **L2** and **C2** overlapped.

Table 2. Cyclic voltammetric potentials (V, vs. Ag/Ag$^+$) of **L2**, **C2** and **Fc**.

Compound	Anodic Potentials E$_{pa}$ (V)	Cathodic Potentials, E$_{pc}$ (V)	
Fc	0.14	0.39	
L2	0.39	0.49	1.33
C2	0.39	0.62	

(Voltammetric scan range −0.600 to +1.60 V). For **Fc** ΔE$_p$ = E$_{pa}$ − E$_{pc}$ = −0.25 V. For **Fc** E$_{1/2}$ = (E$_{pa}$ + E$_{pc}$)/2 = 0.26 V.

Furthermore, the irreversible reduction at E$_{pc}$ = 1.33 V (**B**) assigned to possibly the reduction of the imine nitrogen (C=N), is clearly indicated in Figure 6. **C2** displays a reversible wave at E$_{1/2}$ = 0.50 V (Figure 7) which depicts ferrocene and no further redox activity is observed, which suggests that the palladium centre and the imine nitrogen are stable to redox activity when compared to **L2**. The cyclic voltammograms of **L2** and **C2** are also shown in Figures 7 and 8, respectively.

Figure 7. Cyclic voltammogram of **L2**.

Figure 8. Cyclic voltammogram of **C2**.

Ligand, **L4** (Figure 9), exhibits a voltammogram with a reversible wave at $E_{1/2} = 0.60$ V, assigned to ferrocene followed by three irreversible cathodic peaks at $E_{pc} = 0.9$ V, $E_{pc} = 1.24$ V and $E_{pc} = 1.48$ V. The latter are possibly due to the reduction of the imine nitrogens (**C**, **D** and **E**), although the respective peak assignment is not well understood and may be rearranged for better approximation (Table 3).
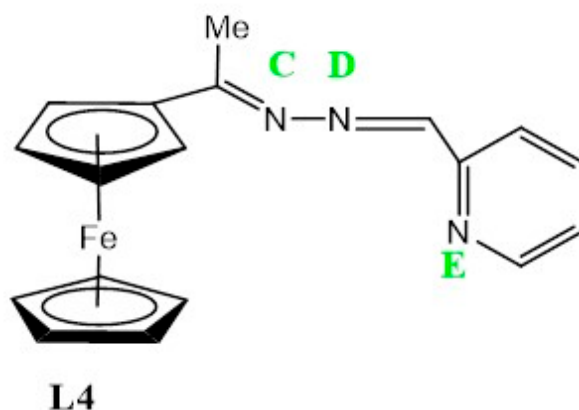

Figure 9. The structure of **L4** with labelled imine nitrogen C-E respectively.

Table 3. Cyclic voltammetric potentials (V, vs. Ag/Ag$^+$) of **L4**, **C4** and **Fc**.

Compound	Anodic Potentials E_{pa} (V)				Cathodic Potentials, E_{pc} (V)
Fc	0.14				0.39
L4	0.45	0.9	1.24	1.48	0.76
C4	0.51				0.65

(Voltammetric scan range −0.600 to +1.60 V). For **Fc** $\Delta E_p = E_{pa} - E_{pc} = -0.25$ V. For **Fc** $E_{1/2} = (E_{pa} + E_{pc})/2 = 0.26$ V.

Upon coordination of **L4** with palladium, **C4** only displays reversible redox activity identified as that of ferrocene at $E_{pa} = 0.51$ V and $E_{pc} = 0.65$ V, thus this complex (**C4**) is more stable as compared to the ligand, as no further redox activity is observed in relation to the imine nitrogen atoms (Figure 10).
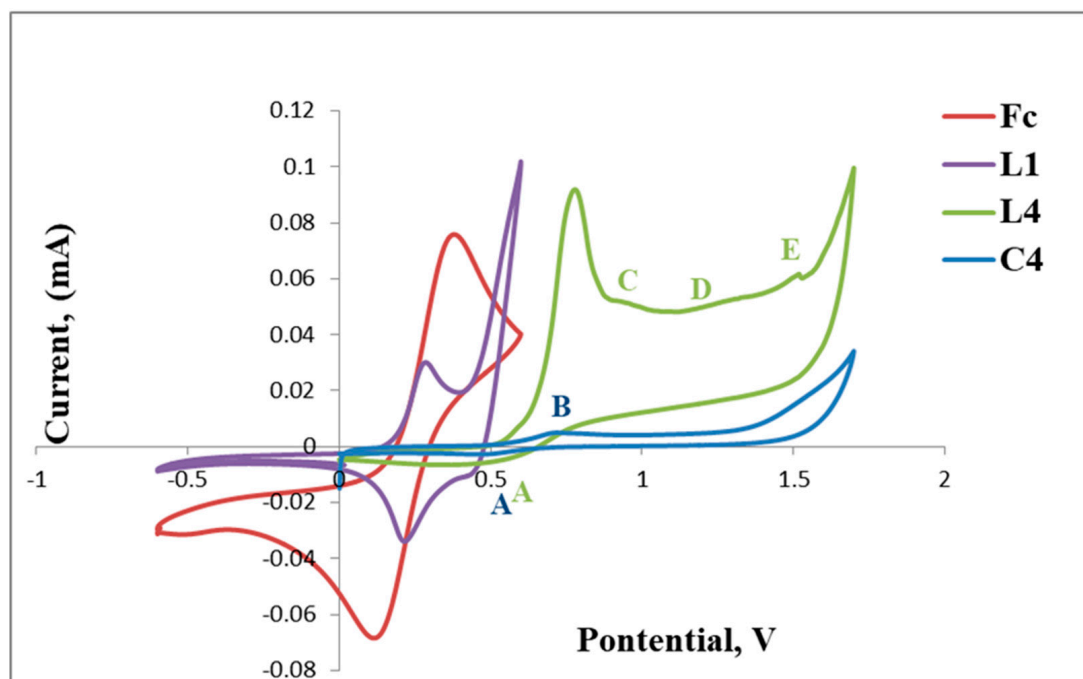

Figure 10. Cyclic voltammograms of ferrocene, **L1**, **L4** and **C4**.

2.4. Mizoroki-Heck Catalytic Studies

2.4.1. Mizoroki-Heck Cross-Coupling Reactions

C1–C4 was employed as catalyst precursors in Mizoroki-Heck cross-coupling reactions, and the optimum reaction conditions were obtained using iodobenzene and styrene as standard substrate models (Figure 11). The solvent, temperature, base, reaction time and catalyst loading were evaluated and established by monitoring the percentage conversion to the optimum.
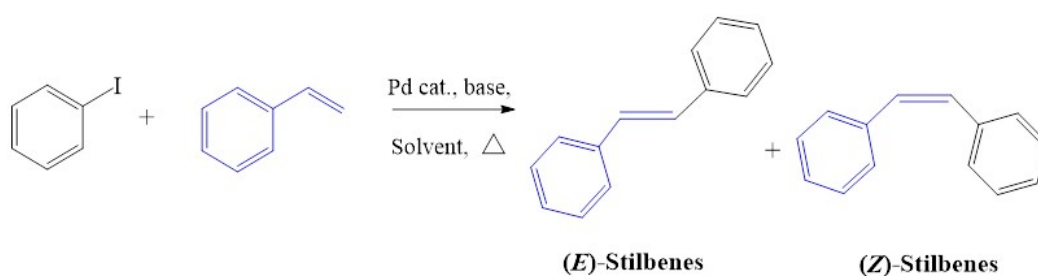

Figure 11. The model substrates used in Mizoroki-Heck reactions, styrene coupled with iodobenzene for the production of (*E*/*Z*) stilbenes.

2.4.2. Optimization of Reaction Conditions for Mizoroki-Heck Cross-Coupling Reactions

The temperature was varied from 80 °C to 140 °C during the cross-coupling of iodobenzene and styrene substrates (Figure S10). Increasing the temperature from 80–100 °C, the percentage conversion of substrates to *cis*- and *trans*-stilbene ranged from 0–75%. Increasing the temperature to 110 °C resulted in increased conversions of **C1** (95%), **C2** (100%), **C3** (100%) and **C4** (91%). Above 110 °C, no significant increase or decrease in conversion was observed for all pre-catalysts, just marginal (95–100%); thus, 110 °C is the optimum temperature. Conversion of the iodobenzene and styrene gave a mixture of two geometric isomers (*trans*- and *cis*-stilbene in a 6:1 ratio), with the (*E*)-stilbene being favoured due to steric reasons, and this has been reported before [7,56–59]. These temperature optimizations were conducted in three solvents: toluene, DMF, and 1,4-dioxane. Reactions in DMF showed better conversions than in toluene (42–62%) and 1,4-dioxane (11–48%). Thus, DMF was found to be the best solvent and used throughout the catalytic evaluations.

The activation of aryl halides often requires the presence of a base [60,61]. Without the use of a base, no activity was observed. Pyridine, sodium methoxide (MeONa) and potassium carbonate (K_2CO_3) were employed but showed no conversions. Triethylamine (Et_3N) and potassium hydroxide (KOH) gave the best conversions, giving up to 100% conversion. In subsequent reactions, triethylamine was used as the base since KOH is highly hygroscopic and difficult to handle. KOH also resulted in drying up the end product(s).

The time it takes for the substrates to be converted to products was also investigated using **C3** as a catalyst precursor. **C3** was selected because it was one of the best performing catalysts during temperature and base optimization, giving ≈100% conversion (TON = 199) at 110 °C with Et_3N (Figures S10 and S11). In the first hour, 78% (*E*)-stilbene was formed exclusively. Upon increasing the reaction time from 1 h to 3 h, a gradual increase in products ((*E*)-stilbene: (*Z*)-stilbene, 85:15) was observed (Figure S12). This decrease suggests that *E*-stilbene is preferably formed initially, and a small amount is then converted to (*Z*)-stilbene over time since no *cis*-isomer was seen in the first hour. After three hours (≈91%), maximum conversions were observed, and beyond 3 h, the conversion did not change much. The turn over frequency (TOF), which is the specific activity of the catalytic centre (Pd) per unit time (h^{-1}), was very high in the first hour (142 h^{-1}, **C3**) but decreased after 3 h to 66 h^{-1} and 61 h^{-1} when using **C3** and **C4** respectively. Furthermore, conversions increased with increasing catalyst loading, and the best conversion was obtained at 0.5 mol% with 100% conversion for **C3**. The optimum conditions, use of Et_3N in DMF with 0.5 mol% at 110°C, favoured **C2** and **C3** to be slightly more efficient, respectively, which may result from the presence of the bulky phosphine facilitating the reaction.

2.4.3. Mercury Poisoning Test

Homogenous catalysis can transform a molecular catalyst into heterogeneous nanoparticles. These heterogeneous nanoparticles are known to contribute towards reactivity by altering homogenous catalyst [62]. However, we did not observe any black palladium particles during optimization reactions, similar to what has been reported in the literature [41,63]. Excitingly, ligands **L1**–**L4** successfully stabilized the palladium(0) active species in the molecular form. In affirmation, the mercury drop (Hg^0) test was conducted, where metallic mercury was added in reaction systems in separate cubes to those without (Table 4). This technique is used to establish true homogeneity of molecular catalysts from heterogeneous (nanoparticle) catalysts [64–66].

Table 4. The results of cross-coupling reactions between iodobenzene and styrene under optimum conditions, and also for the mercury poisoning tests.

Entry	Cat.	Conv. (%)	TON	TOF (hr^{-1})(3 h)	Selectivity (%)		Hg (mg)
					(*E*)-Stilbene	(*Z*)-Stilbene	
1	**C1**	95	189	63	85	15	0
2	**C2**	100	199	66	83	17	0
3	**C3**	100	199	66	87	13	0
4	**C4**	91	183	61	85	15	0
5	**C1**	93	187	62	87	12	1
6	**C2**	98	197	66	83	17	1
7	**C3**	99	198	66	88	12	1
8	**C4**	95	187	62	88	12	1

Notes: Reaction conditions involving coupling of iodobenzene with styrene. Reactions carried out in DMF (1.2 mL) with 0.66 mmol of iodobenzene, 0.726 mmol of styrene, 1.32 mmol of Et_3N and 0.5 mol% Pd catalyst loading using *n*-decane as internal standard and the reaction was allowed to run for 3 h at 110 °C (**C1**–**C4**). Cat. = catalyst, Conv. = conversion. Average error estimates = estimate = **C1** ($\pm$0.3843), **C2** ($\pm$0.1945), **C3** ($\pm$0.2417), **C4** ($\pm$0.2046).

The results from the mercury poisoning tests are presented in Table 4 (entries 1–4; without mercury and entries 5–8; with mercury). There was no significant impact of having metallic mercury in the reactions as seen from the TONs and conversions, which remained high.

2.4.4. Evaluation of Substrate Variation

The palladium pre-catalysts (**C1**–**C4**) were evaluated for their ability to cross-couple substrates with various functional group substituents. These include activated and deactivated aryl halides coupled with substituted styrene and acrylates, respectively.

The deactivated 4-iodotoluene (Figure 12 gave similar results to when iodotoluene was used (Table 5) for pre-catalysts **C1**–**C3** respectively (Table 5, entries 1–4); however, **C4** gave decreased performance of 73% conversion (TON = 148). Similar to iodobenzene, the iodotoulene also favoured the production of *E*-stilbene. We then screened one of the best performing catalyst precursors **C3** in cross-coupling of the activated and deactivated aryl bromides and aryl chlorides with styrene. Surprisingly, the deactivated aryl halides, 4-bromotouene and chlorobenzene gave poor or no conversions ($\approx$0–3%, Table 5 entries 5–8). The activated aryl halides, 2-chlorobenzonitrile (Table 5, entries 9, for **C3**), also gave no conversions. It is possible that the steric demand due to the electron-withdrawing group (NO_2 and CN) being on the *ortho* and *meta* positions of the activated aryl halides affected the catalyst activity since no conversions were observed (Table 5 entries 7 and 9).
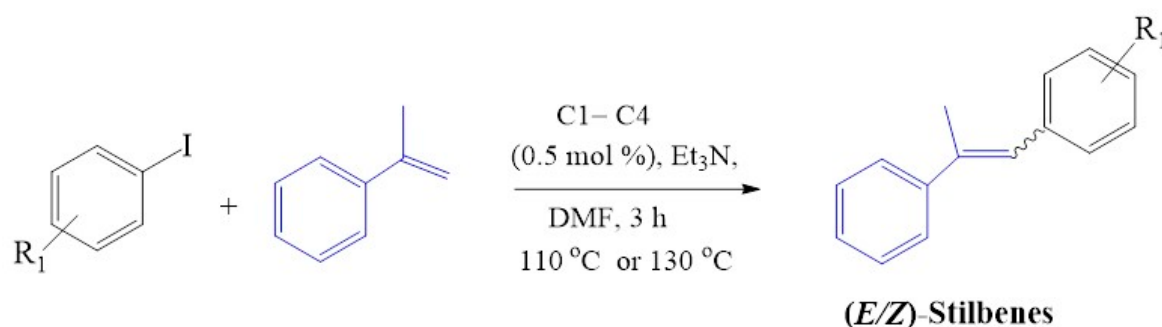
Figure 12. Mizoroki-Heck cross-coupling of activated and inactivated aryl halides with styrene by pre-catalysts **C1–C4**.

Table 5. Mizoroki-Heck cross-coupling of activated and inactivated aryl halides with styrene by pre-catalysts **C1–C4**.

Entry	Cat.	ArX	Conv. (%)	TON	TOF (h^{-1}) (3 h)	Selectivity (%)	
						(*E*)-Stilbene	(*Z*)-Stilbene
1	**C1**		99	199	66	88	12
2	**C2**		95	179	63	88	12
3	**C3**		96	190	64	88	12
4	**C4**		73	148	49	88	12
5	**C3**		2	4	1	–	100
6	**C3**		–	–	–	–	–
7	**C3**		–	–	–	–	–
8	**C3**		3	7	2	–	100
9	**C3**		–	–	–	–	–

Notes: Reactions carried out in DMF (1.2 mL) with 0.66 mmol of iodobenzene/iodotoluene, 0.726 mmol of styrene/α-methyl styrene, 1.32 mmol of Et₃N and 0.5 mol% Pd catalyst loading using *n*-decane as internal standard and the reaction was allowed to run for 3 h at 110 °C (**C1–C4**). Conv. = conversion. Cat. = catalyst. Average error estimate = **C1** (±0.3320), **C2** (±0.3407), **C3** (±0.4721), **C4** (±0.3564).

A significant decrease in product conversions (including TON and TOF) was observed when using pre-catalysts **C1–C4** to couple iodobenzene with sterically hindered α-methyl styrene (Figure 13). The least performance was seen using **C1** and **C4** since both these catalysts gave 19% conversions which correspond to TOFs of 38 and 13 h^{-1}.
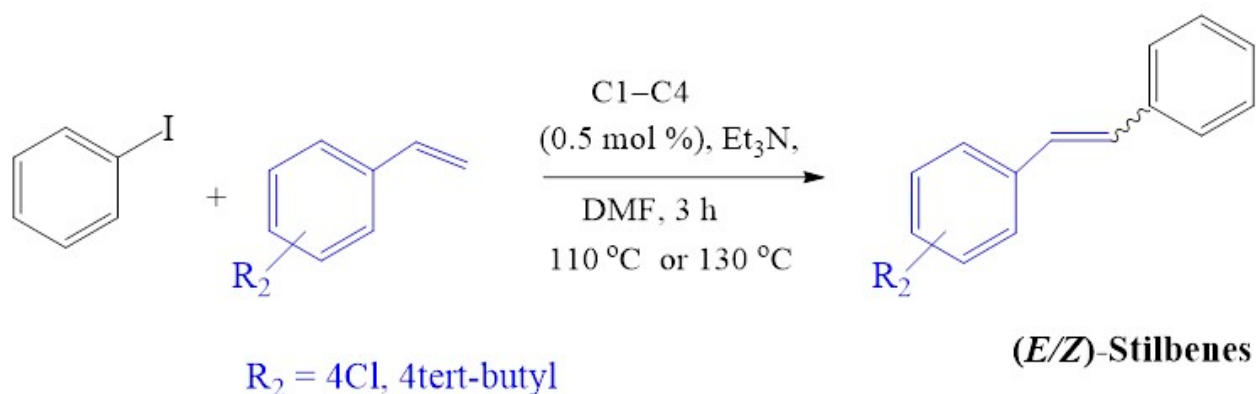
Figure 13. Mizoroki-Heck cross-coupling of iodobenzene with α-methylstyrene using pre-catalysts **C1–C4**.

C1 is a bis(ferrocenyliminehydrazone)palladium(II) catalyst precursors coordinated via primary nitrogen atoms, while **C4** is a bidentate NˆN ferrocenyldiimine palladium(II) catalyst precursor, coordinated to palladium through imine nitrogen atoms. Possibly, the basicity of these ligands leads to lesser stabilization of the active Pd^0 catalysts than with the better π-acceptor iminophosphine and aminophosphine containing catalyst precursors (**C2** and **C3**). The latter catalyst precursors showed better performance (Table 6, entries 2 and 3 compared to those that possess amine and imine donor ligands.

Table 6. Mizoroki-Heck cross-coupling of iodobenzene with α-methylstyrene using pre-catalysts **C1–C4**.

Entry	Cat.	ArX	Conv. (%)	TON	TOF (h^{-1}) (3 h)	Selectivity (%)	
						(*E*)-Stilbene	(*Z*)-Stilbene
1	**C1**		19	38	13	70	30
2	**C2**		48	93	31	82	18
3	**C3**		41	84	28	85	15
4	**C4**		19	38	13	70	30

Notes: Reactions carried out in DMF (1.2 mL) with 0.66 mmol of iodobenzene/iodotoluene, 0.726 mmol of styrene/α-methyl styrene, 1.32 mmol of Et$_3$N and 0.5 mol% Pd catalyst loading using *n*-decane as internal standard and the reaction was allowed to run for 3 h at 110 °C (**C1–C4**). Conv. = conversion. Cat. = catalyst. Average error estimate = **C1** (±0.4926), **C2** (±0.3407), **C3** (±0.6221), **C4** (±0.5414).

The cross-coupling of iodobenzene with the 4-chlorostyrene (Figure 14) using **C1–C4** resulted in good conversions of up to 94% (Table 7, entries 1–4). Cross-coupling of iodobenzene with deactivated 4-tert-butylstyrene resulted in 95–100% conversion (Table 7 entry 5[a] and 8[a]), which is slightly similar when the activated styrene (4-chlorostyrene) was employed (96% and 97%). The *tert*-butyl group provided steric bulkiness, although being further away from the alkene involved in the catalytic transformation, has driven selectivity towards the formation of *E*-stilbenes with some traces of *Z*-stilbenes (*E*:*Z*; ≈ 24:1).
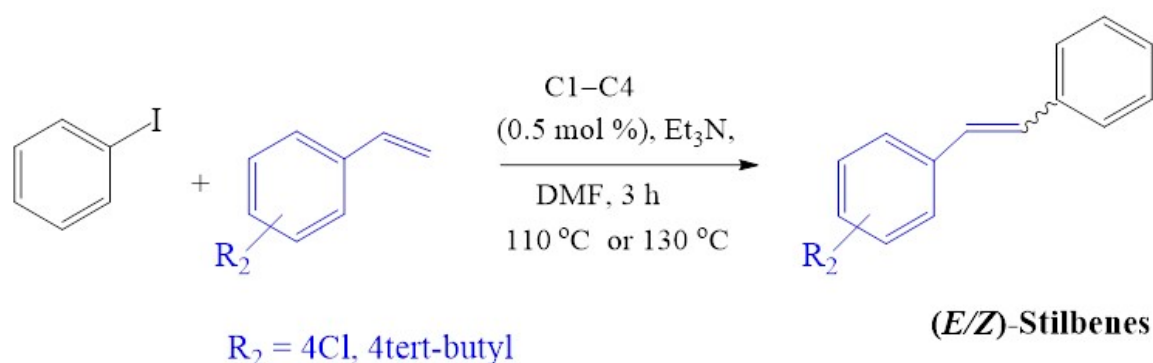
Figure 14. Mizoroki-Heck cross-coupling of iodobenzene with 4-chlorostyrene and 4-tert-butylstyrene using pre-catalysts **C1**–**C4**.

Table 7. Mizoroki-Heck cross-coupling of iodobenzene with 4-chlorostyrene and 4-tert-butylstyrene using pre-catalysts **C1**–**C4**.

Entry	Cat.	ArX	Conv. (%)	TON	TOF (h^{-1}) (3 h)	Selectivity (%)	
						(*E*)-Stilbene	(*Z*)-Stilbene
1	**C1**		94	190	89	84	16
2	**C2**		94	189	63	92	8
3	**C3**		88	177	59	93	7
4	**C4**		93	189	63	90	10
5 [a]	**C1**		97	196	65	96	4
6 [a]	**C2**		100	202	67	96	4
7 [a]	**C3**		95	192	64	99	1
8 [a]	**C4**		95	192	64	95	5

Notes: Reactions carried out in DMF (1.2 mL) with 0.66 mmol of iodobenzene, 0.726 mmol of 4-chlorostyrene or 4-*tert*-butylstyrene, 1.32 mmol of Et₃N and 0.5 mol% Pd catalyst loading using *n*-decane as internal standard and the reaction was allowed to run for 3 h at 110 °C (**C1**–**C4**). Conv. = conversion. Cat. = catalysts. Average error estimate = **C1** (±0.4926), **C2** (±0.5414), **C3** (±0.5161), **C4** (±0.3992). [a] Cross-coupling with 4-methylstyrene as the alkene.

To further extend the scope, Iodobenzene was further coupled to methyl and ethyl acrylates separately using pre-catalysts **C1**–**C4** (Figure 15). These cross-coupling reactions gave 98 to 100% conversions at 0.5 mol% catalyst loading (Table 8, entries 50–63). The trans-isomers (trans-methyl cinnamate and trans-ethyl cinnamate) were favoured (*E*:*Z*: ≈ 40:1). These high conversions demonstrated the catalytic 'system's ability to tolerate functional groups such as esters.
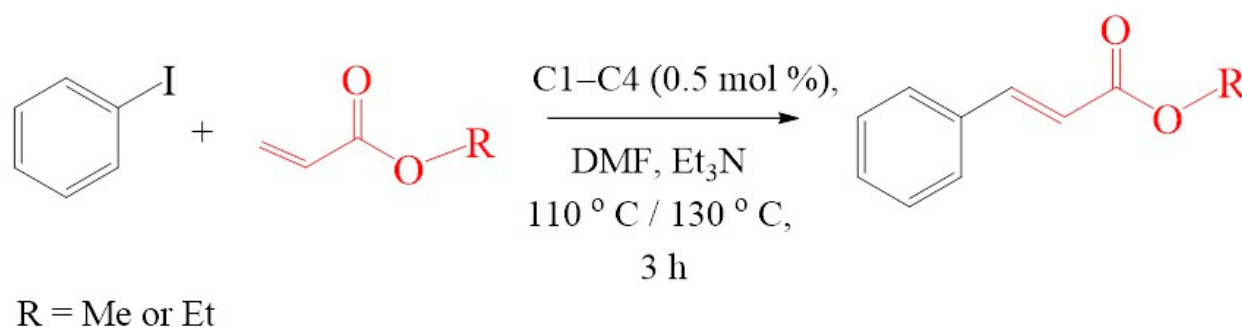
Figure 15. Mizoroki-Heck cross-coupling of iodobenzene with methyl and ethyl acrylates using pre-catalysts **C1–C4**.

Table 8. Mizoroki-Heck cross-coupling of iodobenzene with methyl and ethyl acrylates using pre-catalysts **C1–C4**.

Entry	Cat.	Alkene	Conv. (%)	TON	TOF (h^{-1})	Selectivity (%)	
						(*E*)-Cinnamate	(*Z*)-Cinnamate
1	**C1**	Me	99	202	67	98	2
2	**C2**	Me	99	200	67	98	2
3	**C3**	Me	99	201	67	99	1
4	**C4**	Me	99	201	67	99	1
5	**C1**	Et	100	201	67	98	2
6	**C2**	Et	100	202	67	98	2
7	**C3**	Et	98	197	66	98	2
8	**C4**	Et	99	199	66	98	2

Notes: Reactions carried out in DMF (1.2 mL) with 0.66 mmol of iodobenzene, 0.726 mmol of methyl/ethyl acrylate, 1.32 mmol of Et$_3$N and 0.5 mol% Pd catalyst loading using *n*-decane as internal standard and the reaction was allowed to run for 3 h at 110 °C (**C1–C4**) Cat. = catalysts. Average error estimate = **C1** (±0.3203), **C2** (±0.3407), **C3** (±0.2012), **C4** (±0.3441).

2.4.5. Pre-Catalyst Stability Studies

Stability studies were conducted to evaluate whether the chosen solvent, DMF, does not coordinate with the metal centre during the cross-coupling reactions, contributing to stabilizing the active Pd^0 species responsible for catalysis. **C4** was used as a representative catalyst precursor, where this pre-catalyst was dissolved in DMF-d$_7$ and transferred into an NMR tube, and a ^{1}H-NMR spectrum (Figure 16A) was collected before heating. Another ^{1}H-NMR spectrum was obtained after heating at 110 °C for 3 h (Figure 16B). A slight de-shielding of the aromatic proton signals was observed after heating at 110 °C for 3 h, as was seen from a comparison of spectrum **A** with **B**. Also, a few new peaks shown with the circles were observed, suggesting that the DMF solvent may stabilize the active catalyst in solution during the cross-coupling reactions. Two events may be taking place simultaneously, (1) displacement of the ferrocenylimine ligand to give an in situ generated DMF stabilized species ([Pd(solv)$_4$]) that is represented by the circled peaks on spectrum **A**

and (2) substitution of the chlorido ligands with DMF molecules to give [Pd(**L4**)(solv)$_2$]. Since the chlorido ligands are good π-donor ligands, they give electron density to the palladium resulting in upfield ^{1}H-NMR signals (**B**), while the nitrogen atom in DMF is a good π-acceptor that decreases electron density on palladium, the second event is more likely. This will result in the de-shielding of the ^{1}H-NMR signals (**A**). These stability studies further confirm what was observed during the mercury poisoning tests, that a molecular species is the active catalyst, and the solvent, DMF, likely stabilizes this active species.
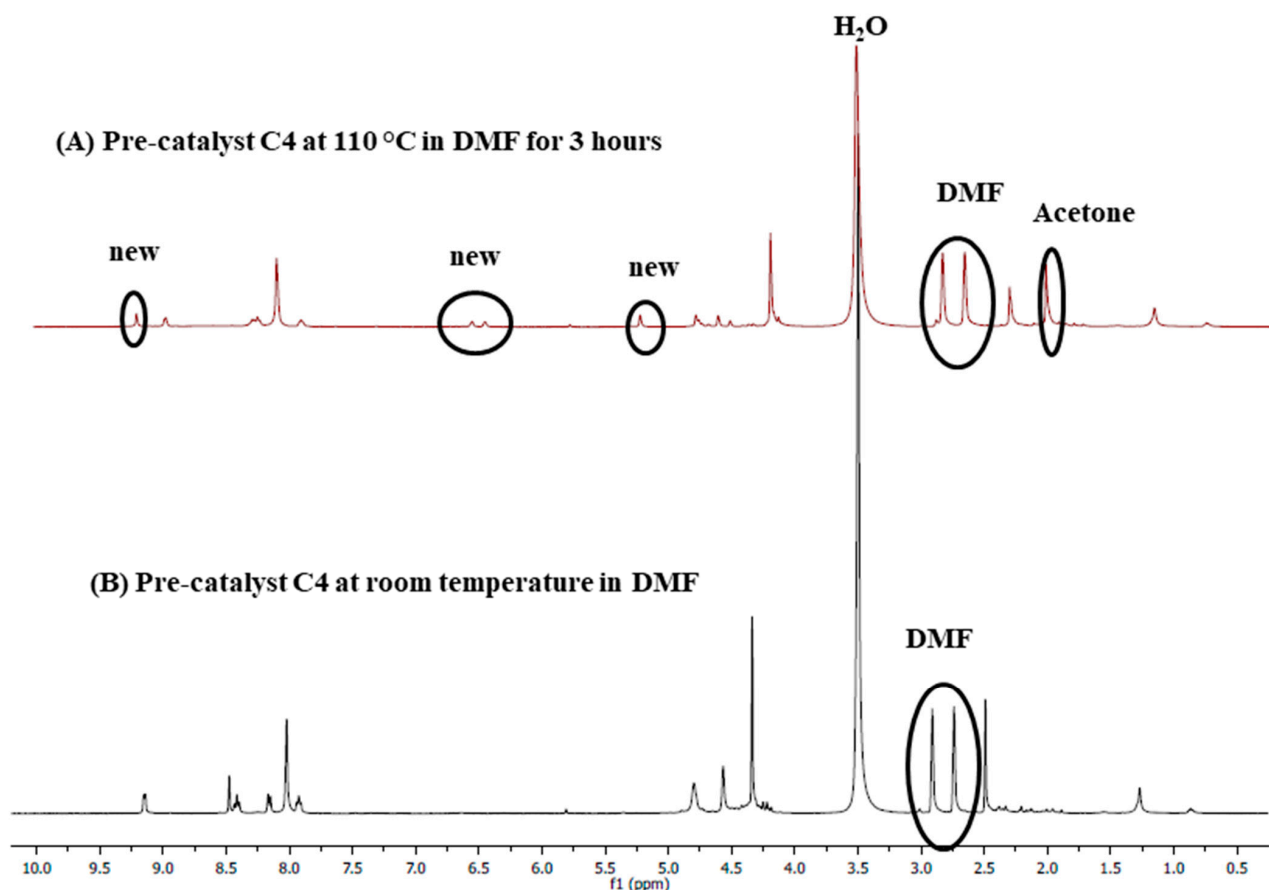

Figure 16. ^{1}H-NMR spectra of **C4** in DMF-d$_7$, (**A**) in DMF-d$_7$ after heating at 110 °C for 3 h. (**B**) at room temperature.

2.5. Computational Studies

Since the mercury poisoning tests and the stability studies suggested molecular Pd^0 catalyst contributions to the Mizoroki-Heck reaction, computational modelling was used to postulate a reaction mechanism when using pre-catalyst **C3** in the cross-coupling reaction of iodobenzene with styrene as model substrates. These mechanistic studies provide essential insights on the activation and oxidative addition of the aryl halide, coordination and insertion of the alkene, β-hydride elimination and dissociation of the coupled product palladium to regenerate the active catalyst.

2.5.1. General Computational Approach to the Mizoroki-Heck Cross-Coupling Reaction

The catalytic pathway of the Mizoroki-Heck cross-coupling reaction proceeds by the formation of an active Pd^0 species. The active species is generated from the pre-catalyst **C3** (Scheme 2). The activation of the pre-catalyst **C3** to Pd^0 is the initial step going into the catalytic cycle. Four steps follow this activation, namely; (1) oxidative addition of the aryl halide (iodobenzene) to the Pd^0 to form a Pd^{II} intermediate, (2) coordination and migratory insertion of the olefin to the Pd^{II} intermediate, (3) β-hydride elimination, which leads to

an intermediate containing a Pd-hydride bond and finally (4) dissociation of the coupled product and reductive elimination of H-Cl and regeneration of the active Pd^0 species.
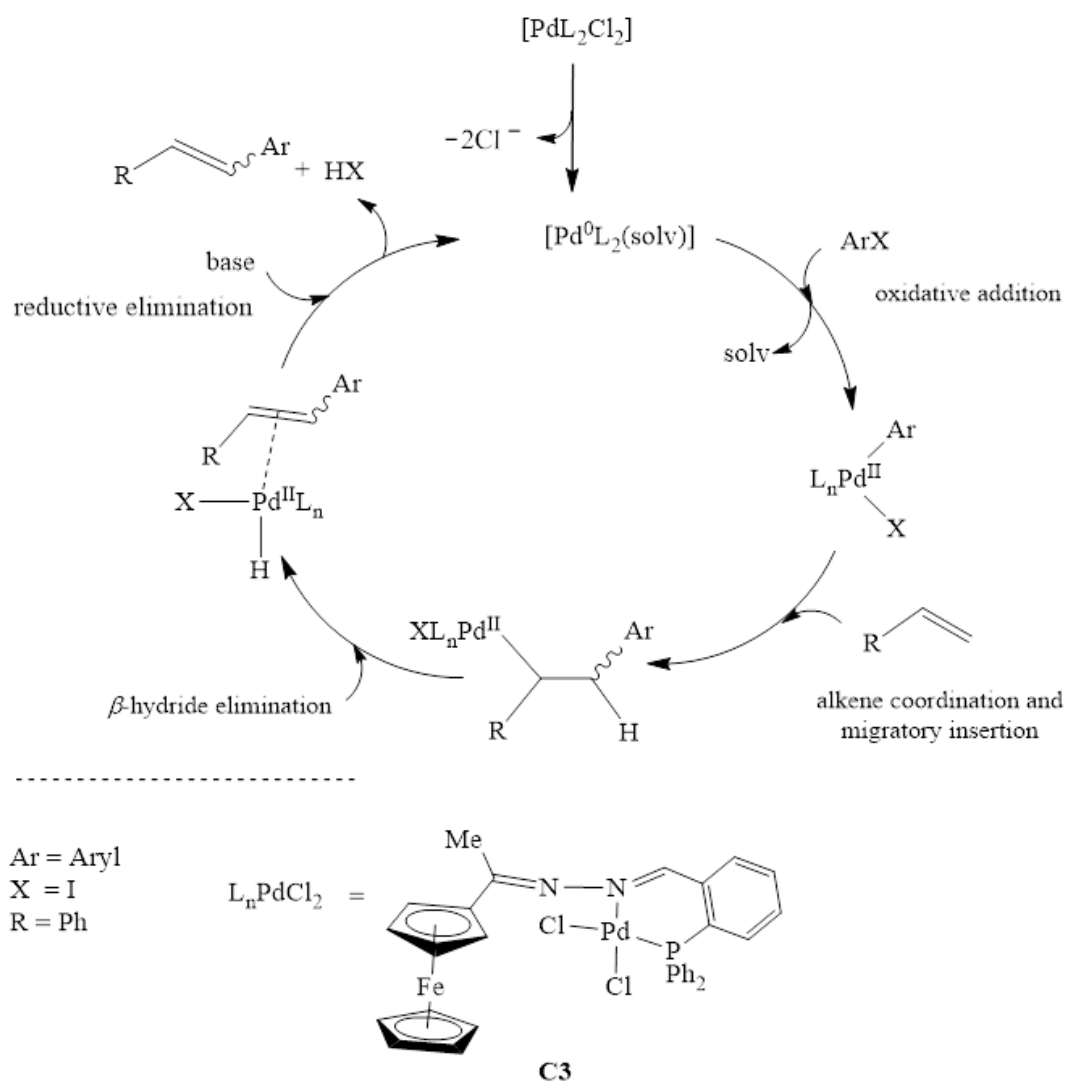
Scheme 2. Catalytic cycle of Mizoroki-Heck carbon-carbon cross-coupling reactions with **C3**.

2.5.2. The Formation of the Active Species, Pd^0L_2

Generation of the active species, Pd^0L_2, can be achieved through cleavage of both the Pd-Cl bonds in **C3**. Cleaving of both the Pd-Cl bonds simultaneously via the concerted approach was investigated. The results revealed that this was not possible because one of the Pd-Cl bonds was longer than the other. Thus, it is the weaker bond and is more likely to first dissociate. According to the *trans*-influence, the bond of a ligand *trans* to a strong σ-donor is weakened due to the better σ-donor contributing more electron density to the 'metals' orbitals than the ligand trans to it [67]. In **C3**, the phosphine is a better σ-donor than the imine nitrogen atom, and it explains why the model found one Pd-Cl bond longer than the other. Thus the weaker Pd-Cl bond is the one trans to the phosphine. Following this finding, we then investigated cleaving Pd-Cl bonds sequentially—one after the other. This was achieved by overcoming a positive activation free energy barrier of 27.4 kcal/mol to afford the transition state **A1TS**, where one chloride ion is leaving (Figure 17).
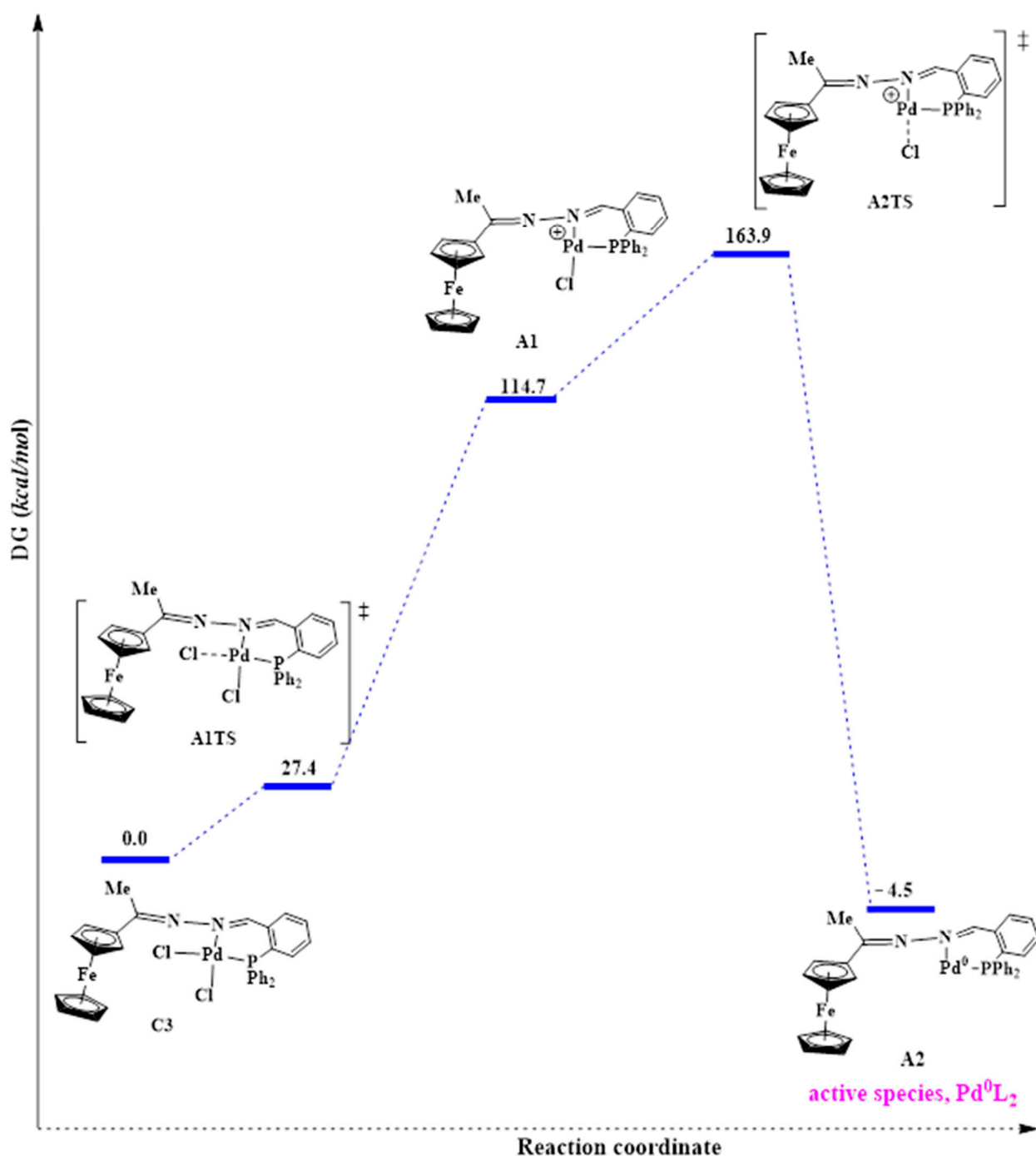
Figure 17. Reaction profile for the proposed pathway leading to the active Pd⁰L₂ species.

However, this was followed by formation of a very unstable intermediate (**A1**) with an energy of 114.7 kcal/mol. The high energy demand (87.3 kcal/mol) for forming this intermediate is possibly why high temperatures (of 110 °C and above) were required, experimentally, to activate this pre-catalyst **C3** during the catalytic testing. The second Pd-Cl bond cleavage had a transition state, **A2TS,** with an even higher energy of 163.9 kcal/mol and was achieved after overcoming an energy barrier of 49.2 kcal/mol. The high energy demands for **A1** and **A2TS** showed that these are extremely unstable and would be difficult to isolate experimentally. Also, since we have seen that the solvent plays a role in stabilizing the active species, the absence of the solvent in the model (calculations conducted in vacuum) means that **A1** and **A2TS** are not solvents stabilized here, and hence

their high energy demand. The active species (**A2**) was associated with a much lower energy of -4.5 kcal/mol and is therefore very stable. This further corroborates that the ligand is effective in stabilizing the Pd^0 active species, and hence it does not decompose to palladium nanoparticles as was seen in the mercury poisoning studies. A huge favourable negative free energy change of -159.4 kcal/mol was required to form **A2**, suggesting a spontaneous reaction.

2.5.3. Oxidative Addition

After forming the active species, Pd^0L_2, the oxidative addition step may proceed by the mono-ligated or bi-ligated approach. The ligation state of the active species is determined by the size of the ligand and may include the bonding nature of the ligand [12,68–70]. In this study, the ligand used was a P^N bidentate ligand which bonded to the palladium centre through phosphorus and nitrogen atoms. We postulated two pathways for the oxidative addition step (Scheme 3): (1) Pathway 1 involved the addition of iodobenzene in a concerted approach. Thus the bonds broke and formed simultaneously; (2) Pathway 2 followed the approach referred to as S_N2 in literature [12,71]. Both pathways revealed that the iodobenzene approaches the Pd^0 centre at a plane almost perpendicular to the {N, Pd, P} coordination plane (Figure 12). In literature, the most common pathway for bidentate systems is that of the concerted approach (Pathway 1) and mostly involves P^P bidentate coordination compounds [69,71]. Interestingly, in this study the concerted approach has not been located, as the concerted transition state (TS) rearranged itself straight into the oxidative addition product. This could mean that, either the TS does not exist (due to unfavourable sterics and/or thermodynamics and kinetics) or it has not been found yet.
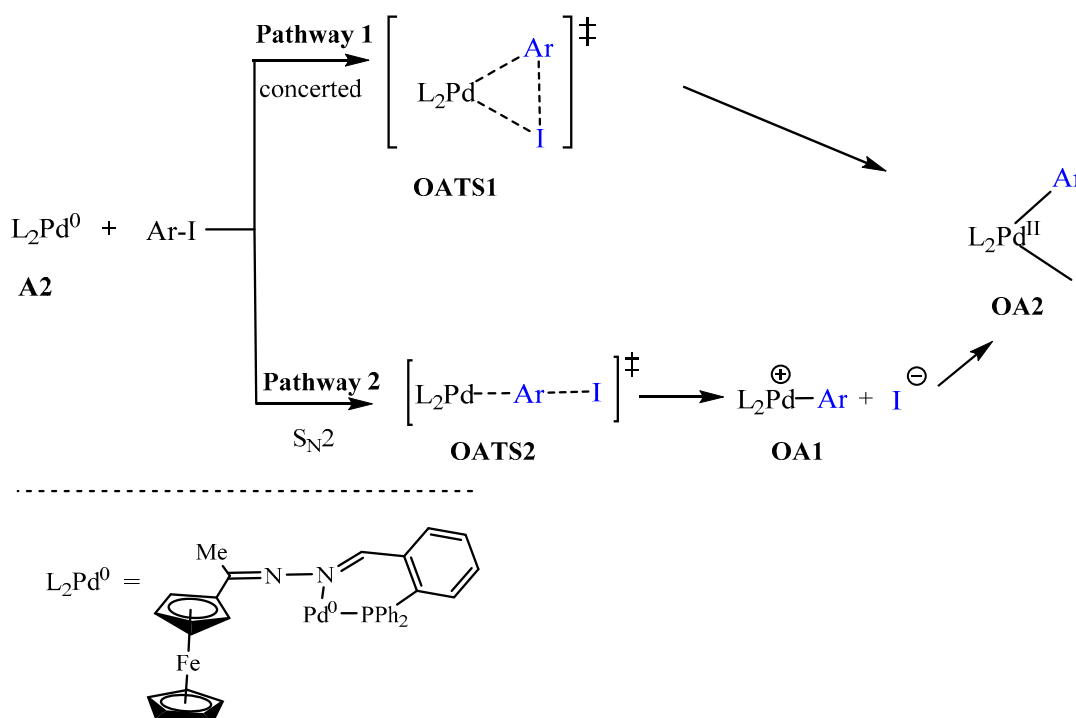
Scheme 3. Possible oxidative addition mechanisms: (**pathway 1**) concerted approach, (**pathway 2**) the S_N2 approach [12,71].

The S_N2 approach is an associative two-step bimolecular process that has been computed successfully in this study following literature protocol [12,71]. Bidentate ligands have been established to direct cis addition of the aryl halide to Pd^0 [69]. The S_N2 transition state (**OATS2**) required an activation energy barrier of -13.2 kcal/mol. The bond distance of Pd-C (in Pd-Ar) was found to be 2.03 Å which was an indication of bond formation. The C-I (in Ar-I) bond distance was equal to 2.63 Å (having lengthened from 2.13 Å). This

was an indication of the C-I bond was breaking. The Pd^0 centre acted as a nucleophile by attacking the electrophilic carbon of the iodobenzene (I-**C**(sp^2)), and the iodide anion was expelled, thus forming an ionic species **OA1** (Figure 18) [12,72]. Subsequently, the iodide anion combined with the charged palladium centre to form **OA2**. **OA1** had an energy barrier −46.2 kcal/mol which was closer to that of **OA2** (−49.1 kcal/mol).
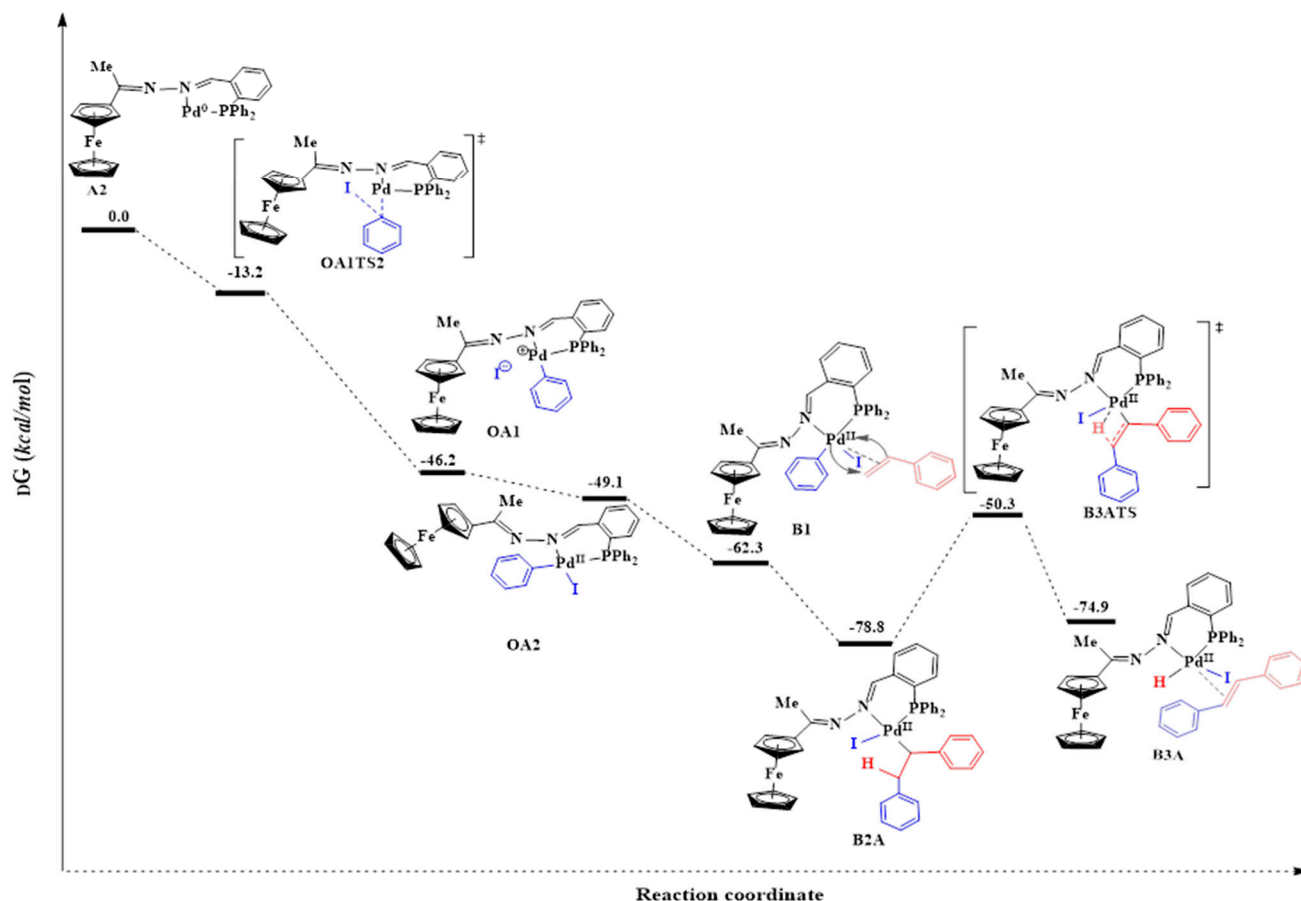

Figure 18. Reaction energy profile for the catalytic steps of the Mizoroki-Heck cross-coupling reaction of iodobenzene with styrene using **C3**.

The addition of the iodobenzene to the Pd^0 to form a Pd^{II} intermediate decreased the bite angle from 101.6° (in **A2**) to 87.8° (in **OA2**) {β ≈ P-Pd-N}. This was an indication of stronger coordination to the palladium centre (Figure 18). The coordination around the Pd^{II} centre in the intermediate **OA2** was square planar, and this was expected for a d^8 heavy metal ion where the chelating ligand has a bite angle of ≈90.0° [73].

2.5.4. Alkene Coordination and Insertion → β-Hydride Elimination

After oxidative addition, styrene was introduced through coordination then insertion into the Pd-C bond in **OA2**. The optimized geometry of **OA2** showed a square planar geometry around the Pd^{II} centre with the ferrocenyl moiety situated below the plane (Figure 19). This implies that the styrene would have approached the complex from above the plane. The 5-coordinate π-complex (**B1**) had favourable free energy of −62.3 kcal/mol, and the olefin approached the square planar palladium plane from below (Figure 18. Prior to the β-hydride elimination step, the phenyl ring (blue) couples with the styrene (red). However, there are two possibilities through which the phenyl ring may couple with the styrene, either following coupling site **A**, Pathway 3, (which ultimately leads to (*E/Z*)-stilbene as the product) or **B**, Pathway 4, (which gives 1,1-diphenylethylene as the product) (Scheme 4). Coupling through site **A** was the most favourable and had free

energy of −78.8 kcal/mol (**B2A**), whereas site **B** required a slightly higher free energy of −76.0 kcal/mol (**B2B**). The energy difference between the two of 2.8 kcal/mol makes **B2A** the most stable, therefore, Pathway 3 has been included in the reaction energy profile (Figure 18). The successive transition state, **B3ATS**, provided evidence that supports that β-hydride elimination occurred following a concerted approach, which requires an imaginary vibrational frequency of at least 100 cm^{-1} for strong vibrations of breaking or forming bonds. A good vibrational frequency of −471 cm^{-1} was obtained for **B3ATS**, as evidence that this transition state was obtained successfully and that it favoured the production of (*E/Z*)-stilbene.
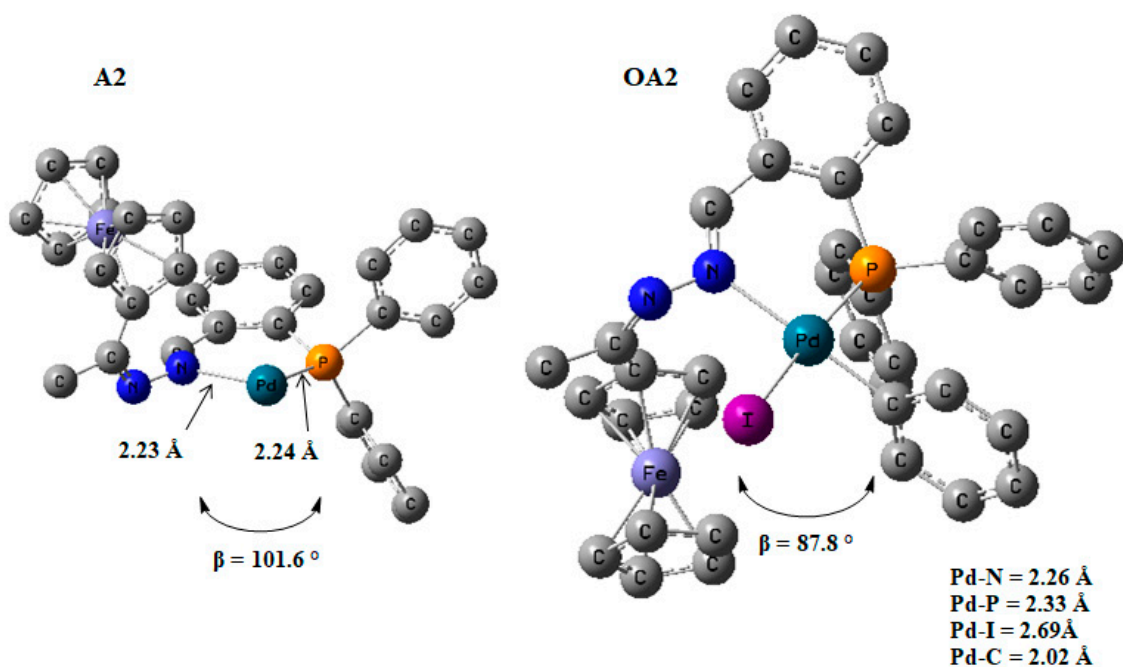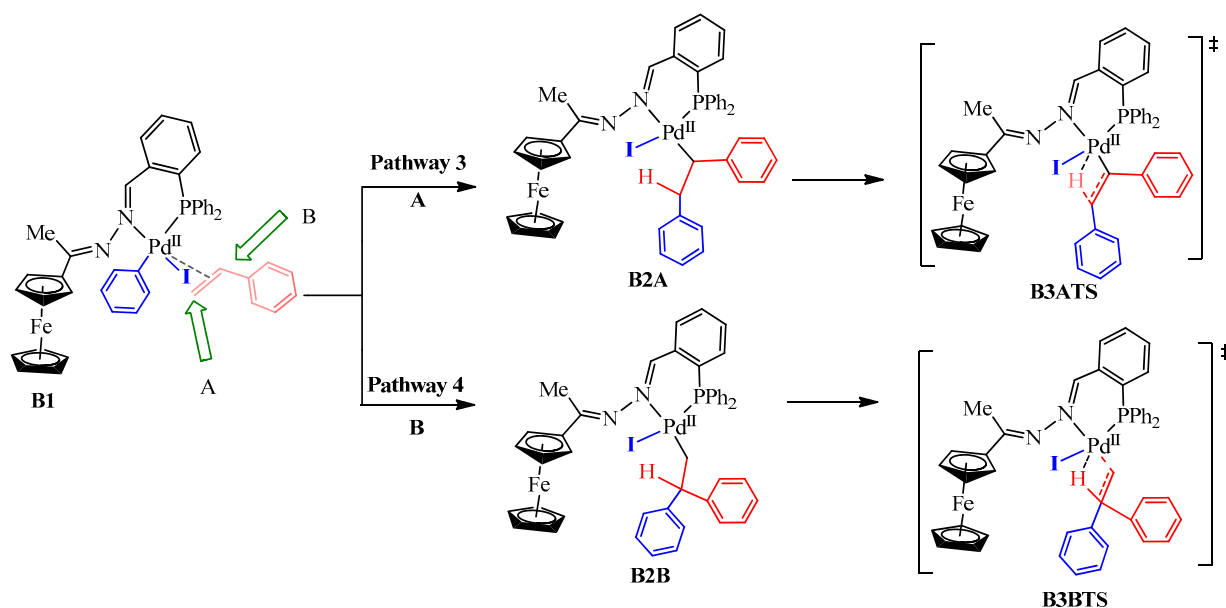

Figure 19. DFT/MO6 optimized geometries of **A2** and **OA2**, β = N-Pd-P angle and bond distance around the palladium centre. Hydrogen atoms omitted for clarity. Hydrogen atoms have been removed.

Scheme 4. Alkene insertion into the Pd^{II} centre of **B1** either at: (**pathway 3**) Site **A** leads to the formation of (*E/Z*)-stilbene; (**pathway 4**) Site **B**, leads to the formation of 1,1-diphenylethylene.

Furthermore, the bond lengths obtained for Pd-H and Pd-C were 1.78 Å and 3.41 Å respectively, and this indicated that the Pd-H bond is forming while the Pd-C bond is breaking in transition **B3ATS** (Scheme 4). B3ATS has a free energy of −50.3 kcal/mol, and **B2A** had to overcome an energy barrier of 28.5 kcal/mol in reaching **B3ATS**. Furthermore, the computational calculations failed to obtain transition state **B3BTS** (Scheme 4), meaning it either does not exist or the model was insufficient to obtain it. Since we did not observe any 1,1-diphenylethylene as one of the cross-coupling products experimentally, the former is more possible.

2.5.5. Reductive Elimination

The reductive elimination step leads to the expulsion of the product together with HI and requires a base. This step regenerates the active Pd^0 species (**A1**), so we investigated the elimination of (*E*/*Z*)-stilbenes bearing in mind that the formation of 1,1-diphenylethylene was ruled out. The 5-coordinate π-complex (**BA3**) where the olefin was E-stilbene was the most stable and favoured. It proceeded through transition state **B3ATS** (−50.3 kcal/mol) and had free energy of −74.9 kcal/mol (Figure 18). The formation of **BA3** comes after a negative free energy change (−24.4 kcal/mol), while a 5-coordinate π-complex (**B3B**) wherein the olefin was Z-stilbene had free energy of 14.7 kcal/mol. This higher energy can be attributed to steric encumbrance between the two phenyl rings in *E*-stilbene (Figure 20).
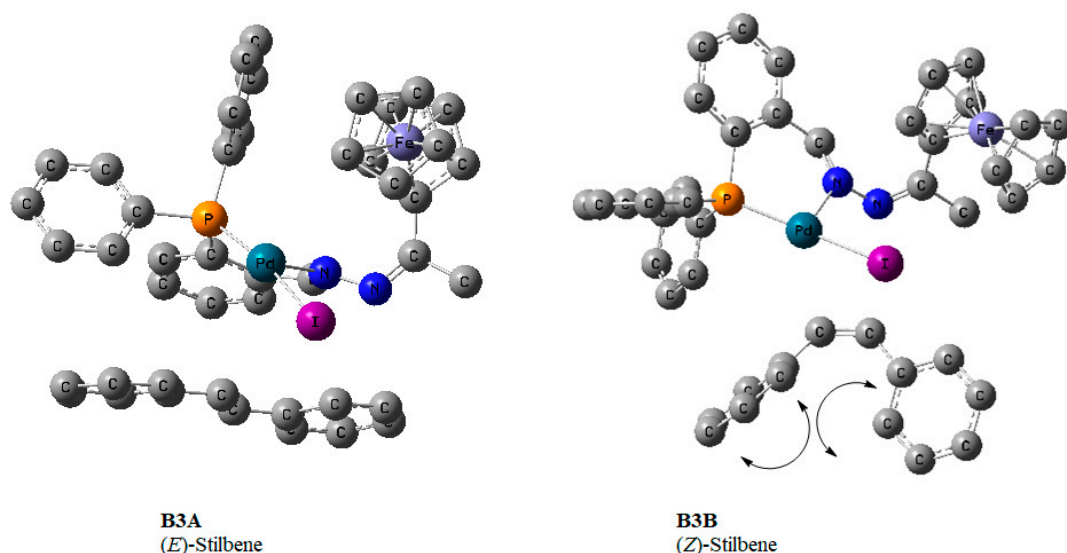

B3A
(*E*)-Stilbene

B3B
(*Z*)-Stilbene

Figure 20. DFT/MO6 optimized geometries of **B3A** and **B3B** showing the *E*- and *Z*-stilbene scenarios, respectively. Hydrogen atoms omitted for clarity. The hydrogen atoms have been removed; this includes the one coordinated directly to the Pd centre.

2.6. Suzuki-Miyaura C-C Cross-Coupling Reactions

Optimization experiments were carried out using bromobenzene and phenylboronic acid as model substrates (Figure 21). As such, temperature, base, reaction time, catalyst loading and solvent were varied with catalyst precursor **C1**–**C4** to establish optimum reaction conditions (Figures S14–S16). As a result, the Suzuki-Miyaura coupling reactions were achieved using these optimum reaction conditions, using DMF solvent, KOH, and 0.5 mol% for 3 h at 150 °C, (Figure S16), and good conversions were obtained under these conditions (Table 7, entries 2–5). Only 37% yield of biphenyl was observed for [Pd(CNMe)$_2$Cl$_2$] under these conditions, and this further emphasized the 'ligands' ability to stabilize the active species better than acetonitrile (Table 9, entry 1).
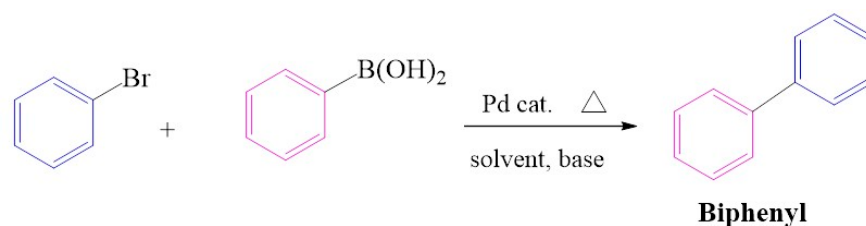
Figure 21. Suzuki-Miyaura coupling of bromobenzene with phenylboronic acid under optimum conditions.

Table 9. Results obtained from Suzuki-Miyaura coupling of bromobenzene with phenylboronic acid under optimum conditions.

Entry	Cat.	Conv. (%)	Selectivity (%)	TON	TOF (h^{-1})
1	[PdCl$_2$(MeCN)$_2$]	37	>99	74	25
2	**C1**	93	>99	188	62
3	**C2**	96	>99	196	63
4	**C3**	87	>99	175	58
5	**C4**	95	>99	189	64

Notes: Reactions carried out in DMF (1.2 mL) with 0.67 mmol of bromobenzene, 1.06 mmol of phenylboronic acid, 1.33 mmol of KOH and 0.5 mol% Pd catalyst loading using *n*-decane as internal standard and the reaction was allowed to run for 3 h at 150 °C (**C1**–**C4**). Conv. = conversion. Cat. = catalyst. Average error estimate = **C1** (±0.5164), **C2** (±0.4132), **C3** (±0.3978), **C4** (±0.4104).

2.6.1. Substrate Variation

Bromobenzene was cross-coupled with ρ-tolylboronic acid, 4-chlorophenylboronic acid and 3, 5-dimethoxyphenylboronic acid using **C1**–**C4** as catalyst precursors (Figure 22). When phenylboronic acid was substituted with a methyl group on the *para*-position, moderate to good percentage conversions were obtained 52–61% (Table 10, entries 1–4). However, this is a decrease in conversions compared to when unsubstituted phenylboronic acid was used (Table 9, entries 2–5). **C2** was more efficient, giving 61% and TON = 197.
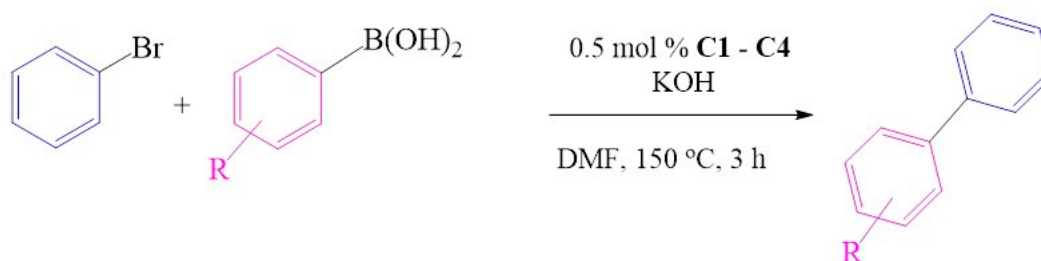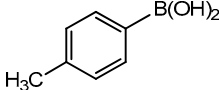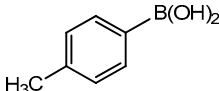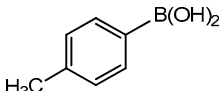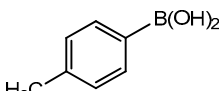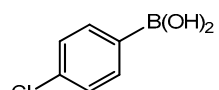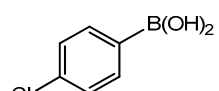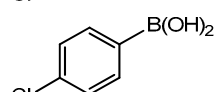

Figure 22. Suzuki-Miyaura coupling of bromobenzene with substituted phenylboronic acid under optimum conditions.

Conversions also decreased when an electron-withdrawing group was on the phenylboronic acid (Table 10, entries 5–9 and Table 11, entries 1–8) as compared to no substituents on the phenylboronic acid substrate (Table 9 entries 2–5), this is possibly because of a decrease in the transmetallation step of the catalytic cycle as has been reported in the literature [16,17,74] The coupling of bromobenzene with 3,5-dimethoxyphenylboronic acid gave slightly improved conversions (Table 11, entries 1–4) in comparison to those with electron-withdrawing group on the phenylboronic acid (Table 11 entries 5–8).

Table 10. Results obtained from Suzuki-Miyaura coupling of bromobenzene with substituted phenylboronic acid under optimum conditions.

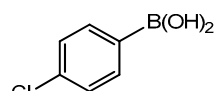| Entry	Cat.	Ph-B(OH)$_2$	Conv. (%)	Selectivity (%)	TON	TOF(h^{-1})
1	**C1**		56	>99	113	38
2	**C2**		61	>99	123	41
3	**C3**		52	>99	105	35
4	**C4**		56	>99	114	38
5	**C1**		52	98	106	35
6	**C2**		51	99	104	34
7	**C3**		51	100	103	34
9	**C4**		54	100	108	36

Notes: Reactions carried out in DMF (1.2 mL) with 0.67 mmol of bromobenzene, 1.06 mmol of substituted phenylboronic acid (X = 4-CH$_3$ and 4-Cl), 1.33 mmol of KOH and 0.5 mol% Pd catalyst loading using *n*-decane as internal standard and the reaction was allowed to run for 3 h at 150 °C (**C1**–**C4**). Conv. = conversion. Cat. = catalyst. Average error estimate = **C1** ($\pm$0.3351), **C2** ($\pm$0.4067), **C3** ($\pm$0.3412), **C4** ($\pm$0.2975).

Furthermore, the observed marginal improvement in conversions are possibly due to the methoxy groups being on the meta-positions (and they are therefore electron-withdrawing) rather than in the *para*-position. The methoxy group is electron-withdrawing by the inductive effect of the oxygen atom, (electronegativity of oxygen is 2.6) however, in the *para*-position, the availability of lone pair of electrons on the oxygen can undergo back donation into the aromatic ring by resonance giving rise to an additional resonance structure [75]. Therefore, the *para*-methoxy substituent is an electron-donating group, even though the same group is electron-withdrawing in the *meta*-position.

In 3,5-dimethoxyphenylboronic acid, there are two moderately electron-withdrawing groups which result in slightly improved conversions. When 4-formylphenylboronic acid and 3-nitrophenylboronic acid were used as substrates, the weakly electron-withdrawing formyl on the phenylboronic acids resulted in marginally different conversions as compared to the more electron-withdrawing nitro substituent on the phenylboronic acid (Table 12 entries 5–8 and Table 13 entries 1–4). These reactions also proved no homo coupling when 4-formylphenylboronic acid was used and less than 1% homo coupling revealed for 3-nitrophenylboronic acid.

Table 11. Results obtained from Suzuki-Miyaura coupling of bromobenzene with substituted phenylboronic acid under optimum conditions.

Entry	Cat.	Ph-B(OH)₂	Conv. (%)	Selectivity (%)	TON	TOF(h⁻¹)
1	**C1**	MeO / OMe phenylboronic acid	69	100	139	46
2	**C2**	MeO / OMe phenylboronic acid	70	>99	140	47
3	**C3**	MeO / OMe phenylboronic acid	53	>99	113	38
4	**C4**	MeO / OMe phenylboronic acid	65	>99	131	43
5	**C1**	OHC phenylboronic acid	28	100	57	19
6	**C2**	OHC phenylboronic acid	30	100	62	20
7	**C3**	OHC phenylboronic acid	66	100	134	44
8	**C4**	OHC phenylboronic acid	19	100	38	12

Notes: Reactions carried out in DMF (1.2 mL) with 0.67 mmol of bromobenzene, 1.06 mmol of substituted phenylboronic acid (4-CHO and 3,5-diMeO), 1.33 mmol of KOH and 0.5 mol% Pd catalyst loading using *n*-decane as internal standard and the reaction was allowed to run for 3 h at 150 °C (**C1–C4**). Conv. = conversion. Cat. = catalyst. Average error estimate = **C1** (±0.5643), **C2** (±0.6413), **C3** (±0.3820), **C4** (±0.5001).

Table 12. Results obtained from Suzuki-Miyaura coupling of bromobenzene with substituted phenylboronic acid under optimum conditions.

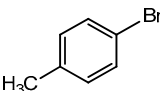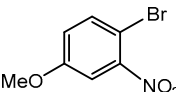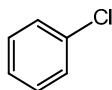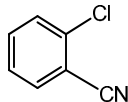| Entry	Cat.	Ph-B(OH)₂	Conv. (%)	Selectivity (%)	TON	TOF (h⁻¹)
1	**C1**	NO₂ phenylboronic acid	41	>99	83	28
2	**C2**	NO₂ phenylboronic acid	53	>99	107	36
3	**C3**	NO₂ phenylboronic acid	45	>99	91	30
4	**C4**	NO₂ phenylboronic acid	48	>99	98	33

Notes: Reactions carried out in DMF (1.2 mL) with 0.67 mmol of bromobenzene, 1.06 mmol of substituted phenylboronic acid (X = 4-CO₂H, 3-NO₂), 1.33 mmol of KOH and 0.5 mol% Pd catalyst loading using *n*-decane as internal standard and the reaction was allowed to run for 3 h at 150 °C (**C1–C4**). Conv. = conversion. Cat. = catalyst. Average error estimate = **C1** (±0.4310), **C2** (±0.2431), **C3** (±0.3634), **C4** (±0.3043).

Table 13. Results obtained from Suzuki-Miyaura cross-coupling of activated and deactivated aryl halides with phenylboronic acid.

Entry	Cat.	ArX	Conv. (%)	Selectivity (%)	TON	TOF (h^{-1})
1	**C3**		68	93	137	46
2	**C3**		100	77	202	67
3	**C3**		32	100	65	22
4	**C3**		81	>99	163	54

Notes: Reactions carried out in DMF (1.2 mL) with 0.67 mmol of substituted aryl halide, 1.06 mmol phenylboronic acid, 1.33 mmol of KOH and 0.5 mol% Pd catalyst loading using *n*-decane as internal standard and the reaction was allowed to run for 3 h at 150 °C (**C3**). Conv. = conversion. Cat. = catalyst. Average error estimate **C3** (±0.3266).

The substrate scope of the aryl halide was studied using (pre)catalyst **C3**, and the activated aryl halides gave better conversions than the deactivated aryl halides (Table 13, entries 1–4). The presence of electron-withdrawing groups resulted in excellent conversion (Table 13, entries 2 and 4), while having an electron-donating group on bromobenzene resulted in moderate conversions of up to 68% (Table 13, entry 1). In addition, having a methoxy group on the para- position and a nitro group on the ortho-position did not affect the reaction sterically or stereo-electronically as was seen from the 100% conversion that this reaction gave (Table 13, entry 3). The activated aryl chloride (2-cyanochlorobenzene) gave a good conversion to the corresponding biphenyl and excitingly, the cross-coupling of deactivated aryl chloride with phenyl boronic acid gave 32% conversions (Table 13, entry 1).

2.6.2. Mercury Poisoning Test

The homogeneity test was performed for (pre)catalysts **C1**–**C4** under the optimal conditions by adding metallic mercury to the reactions vessels respectively. A significant drop in conversion by ≈50% was observed. This indicates that a "cocktail" of catalysts may be accountable for the reactions where some of the pre-catalyst forms nanoparticles and the molecular catalysts are also present during the reactions [76].

3. Materials and Methods

3.1. General Information

All experiments were conducted in air unless otherwise stated. Solvents used were reagent grade and were not distilled before use unless otherwise stated. All chemicals were purchased from Sigma Aldrich (Johannesburg warehouse, Johannesburg, South Africa) and used as received. However, the solvents were kept anhydrous in molecular sieves. These include hydrazine monohydrate, ferrocenyl methyl ketone, chlorodiphenylphosphine, 2-diphenylphosphino benzaldehyde, 2-pyridine carboxaldehyde, triethylamine and other chemicals used herein. PdCl$_2$ was purchased from Heraeus (Boksburg, South Africa) and used as received. [PdCl$_2$(MeCN)$_2$] was synthesized according to literature procedures [77]. ^{1}H-NMR were recorded on a 400 MHz (^{1}H at 400 MHz, ^{13}C{^{1}H} at 100 MHz and ^{31}P{^{1}H} at 162 MHz instrument (Bruker, Johannesburg, South Africa). The chemical shift values were reported relative to the internal standard tetramethylsilane (δ 0.00). These were referenced to the residual proton and carbon signals at 7.24 and 77.0 ppm, respectively, of CDCl$_3$.

Similarly for DMSO-d_6, the reference for the residual proton and carbon signals at 2.49 and 39.0 ppm, respectively. Analytical thin-layer chromatography (TLC) was

performed using silica gel coated aluminium plates (0.2 mm). Developed plates were then analyzed through visualization under the UV light or iodine staining. Silica gel column chromatography was performed using silica gel 60 (70–230 mesh). FT-IR spectra (between 4000–600 cm^{-1}) were recorded as ATR using a BX (II) spectrometer (Perkin Elmer, Midrand, South Africa). Elemental analyses were conducted using a Flash 2000 CNHSO analyzer (Thermo Scientific, Corston, UK). ESI-MS was carried out at Stellenbosch University Central Analytical Services using a Synapt G2 system (Stellenbosch, South Africa) and melting points were determined using a Digital Melting-point Apparatus 5A 6797 (Gallenkamp, Prinses Beatrixlaan, The Netherlands). XRD spectra were obtained from a Bruker APEX-II CCD Diffractometer.

3.2. Synthesis and Characterization of Ligands, *L1–L4*

3.2.1. Preparation of Ferrocenyl Methyl Hydrazone Ligand, **L1**

L1 (Figure 23) was synthesized via a Schiff base reaction of acetylferrocene (1.90 g, 0.00833 mmol) with an excess of hydrazine monohydrate (0.854 g, 0.0266 mmol) followed by the addition of 2–4 drops of acetic acid in ethanol (50 mL). The reaction solution was refluxed for 6 h at 85 °C. The solvent was then removed, and the resultant precipitate was collected and dried under vacuum for 5 h. An orange solid was isolated. Yield: 2.02 g, 97%. Melting point: 110–113 °C (literature) [33]: 110–114 °C). FT-IR (ν_{max}/cm^{-1}): 3200 (N-H), 1600 ν(C=N). ^{1}H-NMR (DMSO-d_6): δ ppm = 1.92 (s, 3H, H$_b$), 4.10 (s, 5H, H$_g$), 4.20 (s, 2H, H$_f$), 4.44 (s, 2H, H$_e$), 5.83 (br s, 2H, H$_a$). ^{13}C{^{1}H}-NMR (DMSO-d_6): δ ppm = 12.7 (C$_b$), 65.6 (C$_g$), 68.3 (C$_e$), 79.2 (C$_f$), 80.5 (C$_d$), 159.4 (C$_c$). Elemental Analysis (Calculated % for C$_{12}$H$_{14}$FeN$_2$): C 59.53, H 5.83, N 11.57. Found %: C 59.96, H 6.16, N 11.89. ESI-MS(+): m/z = 242.0506 [M]$^+$.
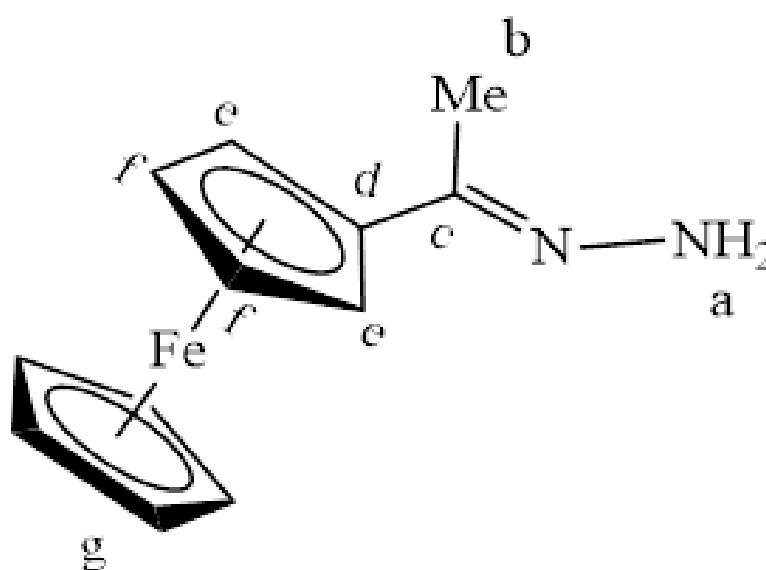
L1

Figure 23. The chemical structure of **L1**.

3.2.2. Preparation of Ferrocenyl Aminophosphine Ligand, **L2**

L1 (0.150 g, 0.616 mmol) was dissolved in dry THF, and triethylamine (0.0620 g, 0.616 mmol) was added. The mixture was allowed to stir at room temperature for 30 min to deprotonate one of the amino protons. Chlorodiphenylphosphine (0.136 g, 0.616 mmol) was added under nitrogen gas, and the solution was stirred for 24 h at 0–5 °C. After 24 h,

the solution was washed with distilled water (20 mL) about five times. The DCM layer was then collected, dried over anhydrous magnesium sulfate, and the solvent was removed using a rotary evaporator. The remaining maroon solid of L2 (Figure 24) was further dried under vacuum for 8 h. Yield: 0.118 g, 45%. Melting point: decomposes without melting; onset occurs at 146 °C. FT-IR (ν_{max} /cm^{-1}): 3102 (N-H), 1596 (C=N). ^{1}H-NMR (DMSO-d_6) δ ppm = 2.11 (s, 3H, H$_f$), 4.16 (br m, 5H, H$_a$), 4.39 (s, 1H, H$_b$) and 4.55 (s, 1H, H$_{b''}$), 4.71 (d, ^3J = 4.74 Hz, 2H, H$_c$), 7.36–7.57 (br m, 7H, H$_{j,g}$), 7.82 (br m, 4H, H$_i$). ^{13}C{^{1}H}-NMR (CDCl$_3$): δ ppm = 15.7 (C$_f$), 67.3 (C$_g$), 69.2 (C$_a$), 69.9 (C$_c$), 83.7 (C$_d$), 128.5 (C$_i$), 131.8 (C$_j$), 132.5 (C$_h$), 158.8 (C$_e$). ^{31}P{^{1}H}-NMR (DMSO-d_6): δ = 23.6 ppm. Elemental Analysis (Calculated % for C$_{24}$H$_{23}$FeN$_2$P): C 67.62, H 5.44, N 6.57. Found %: C 67.33, H 5.16, N 6.13. ESI-MS(+): m/z = 453.0724 [M+Na]$^+$.
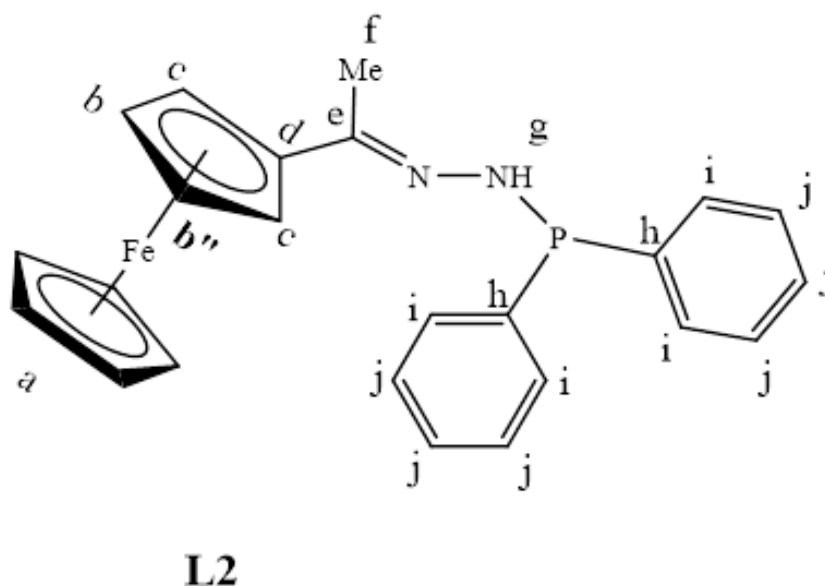

L2

Figure 24. The chemical structure of **L2**.

3.2.3. Preparation of Ferrocenyl(Diphenylphosphine)Phenylimine Ligand, **L3**

L1 (0.834 g, 0.00344 mmol) was dissolved in dry EtOH (30 mL) and 2-diphenylphosphine benzaldehyde (1.00 g, 0.00344 mmol) was added. The solution was refluxed at 85 ° C for 24 h to achieve a Schiff base condensation reaction. The solvent was then removed using a rotary evaporator and a red precipitate of L3 (Figure 25) was obtained. This was then dried under vacuum for 5 h. Yield: 0.00156 g, 88%. Melting point: 62–64 °C. FT-IR (ν_{max}/cm^{-1}): 1555 (C=N) and 1607 (C=N). ^{1}H-NMR (DMSO-d_6): δ ppm = 2.16 (s, 3H, H$_m$), 4.13 (s, 5H, H$_q$), 4.43 (s, 2H, H$_o$), 4.70 (s, 2H, H$_p$), 6.79 (br s, 1H, H$_f$), 7.19 (br s, 2H, H$_a$), 7.52 (br s, 4H, H$_b$), 7.63 (br m, 4H, H$_c$), 8.05 (br s, 1H, H$_i$), 8.71 (br s, 1H, H$_k$). ^{13}C{^{1}H}-NMR (DMSO-d_6): δ ppm = 15.9 (C$_m$), 67.7 (C$_p$), 69.0 (C$_q$), 70.4 (C$_o$), 81.9 (C$_n$), 127.4–128.0 (br m,C$_{a,b,g,h}$), 130.3 (C$_c$), 133.4 (C$_f$),135.1 (C$_i$) 136.3 (C$_j$), 154.4(C$_e$), 154.6 (C$_d$), 157.8(C$_k$), 167.1 (C$_l$). ^{31}P{^{1}H}-NMR (DMSO-d_6): δ ppm = −13.1. Elemental Analysis (Calculated % for C$_{31}$H$_{27}$FeN$_2$P): C 72.38, H 5.29: N 5.45. Found: C 72.11, H 5.26, N 5.48. ESI-MS(+): m/z = 515.1346 [M + H]$^+$.
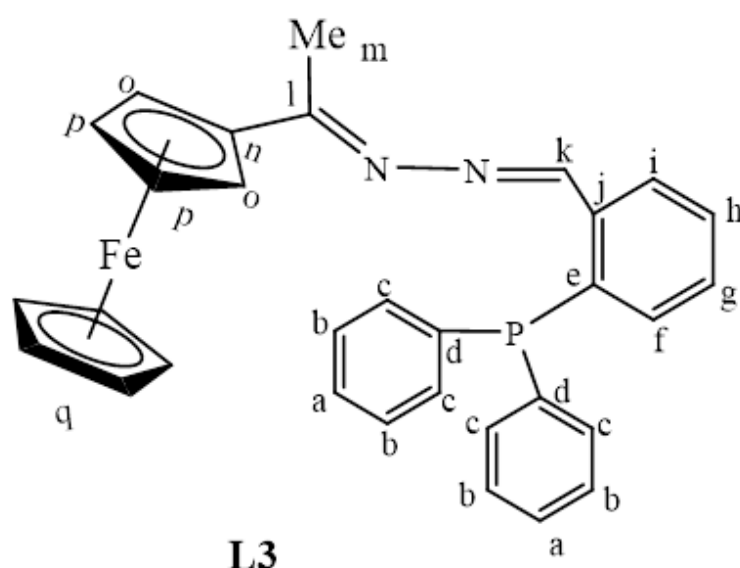
Figure 25. The chemical structure of **L3**.

3.2.4. Preparation of Ferrocenyl(Pyridyl)imine Ligand, **L4**

2-Pyridine carboxaldehyde (0.150 g, 0.619 mmol) was added to a solution of **L1** (0.666 g, 0.616 mmol) in ethanol (30 mL). The solution was refluxed for 48 h at 85 °C. After 48 h, the solvent was removed by rotary evaporation, and a sticky red solid was obtained. The TLC revealed a mixture of products but mainly unreacted **L1** and the desired product. Column chromatography was used to separate the mixture of **L1** and **L4** using ethyl acetate and hexane (3:1) as an eluent. **L1** eluted first, followed by **L4**. **L4** contained trace amounts of 2-pyridine carboxaldehyde extracted into deionized water by washing a DCM (30 mL) solution of **L4** and 2-pyridine carboxaldehyde with deionized water (30 mL) three times. The DCM layer was then collected, dried over anhydrous magnesium sulfate, and the DCM solvent was removed by using a rotary evaporator. **L4** (Figure 26) was isolated as a sticky red solid, which was dried under vacuum for 6 h. Yield: 0.170 g, 42%. Melting point: 73–75 °C. FT-IR (ν_{max}/cm^{-1}): 1566, 1588, 1613(C=N). ^{1}H-NMR (DMSO-d_6): δ ppm = 2.36 (s, 1H, H_h), 4.22 (m, 5H, H_l), 4.48 (s, 2H, H_k), 4.79 (s, 2H, H_j), 7.45 (t, ^3J = 7.5 Hz, 1H, H_c), 7.88 (t, ^3J = 7.9 Hz, 1H, H_b), 8.08 (d, ^3J = 8.1 Hz, 1H, H_d), 8.29 (s, 1H, H_f), 8.65 (br d, ^3J = 8.7 Hz, 1H, H_a). ^{13}C{^{1}H}-NMR (DMSO-d_6): δ ppm = 16.3 (C_h), 68.0 (CH_{Fc}), 69.5 (CH_{Fc}), 70.0 (CH_{Fc}), 81.4 (C_i), 120.5 (C_d), 124.3 (C_b), 136.3 (C_c), 149.2 (C_a), 152.8 (C_e), 155.6 (C_f), 167.1 (C_g). Elemental Analysis (Calculated % for $C_{24}H_{26}Cl_2Fe_2N_4Pd$): C 65.28, H 5.17, N 12.69. Found %: C 65.42, H 5.06, N 12.47. ESI-MS(+): m/z = 332.0858 [M + H]$^+$.
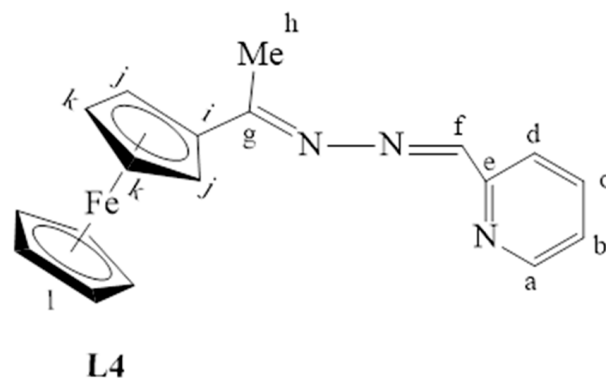

Figure 26. The chemical structure of **L4**.

3.3. Synthesis and Characterization of Complexes, *C1–C4*

3.3.1. Synthesis of [PdCl$_2$(**L1**)$_2$], **C1**

L1 (0.400 g, 1.652 mmol) was dissolved in 30 mL DCM followed by the addition of *bis*(acetonitrile)dichloropalladium(II) (0.214 g, 0.826 mmol) and this solution was stirred at room temperature for 72 h. The resulting purple suspension was obtained by gravity filtration was washed with DCM (5 mL × 2) and diethylether (15 mL × 5). The precipitate **C1** (Figure 27) was then dried under vacuum for 2 h. Yield: 0.547 g, 100%. Melting point: decomposes without melting, onset occurs at 198 °C. FT-IR (ATR, ν_{max}/cm^{-1}): 3094 (N-H), 1606 ν(C=N). ^{1}H-NMR (DMSO-d_6): δ ppm = 2.42 (s, 6H, H$_f$), 4.23 (br s, 10H, H$_a$), 4.38 (br s, 4H, CH$_{Fc}$), 4.67 (br s, 4H, CH$_{Fc}$), 7.46 (br s, 4H, H$_g$). ^{13}C{^{1}H}-NMR (DMSO-d_6): δ ppm = 16.5 (C$_f$), 66.8 (CH$_{Fc}$), 68.9 (C$_a$), 69.7 (CH$_{Fc}$), 82.5 (C$_d$), 174.3(C$_e$). Elemental Analysis (Calculated % for C$_{24}$H$_{26}$Cl$_2$Fe$_2$N$_4$Pd): C 43.71, H 3.97, N 8.50. Found %: C 43.79, H 4.01, N 8.39. ESI-MS(+): m/z = 622.9710 [M-Cl]$^+$.
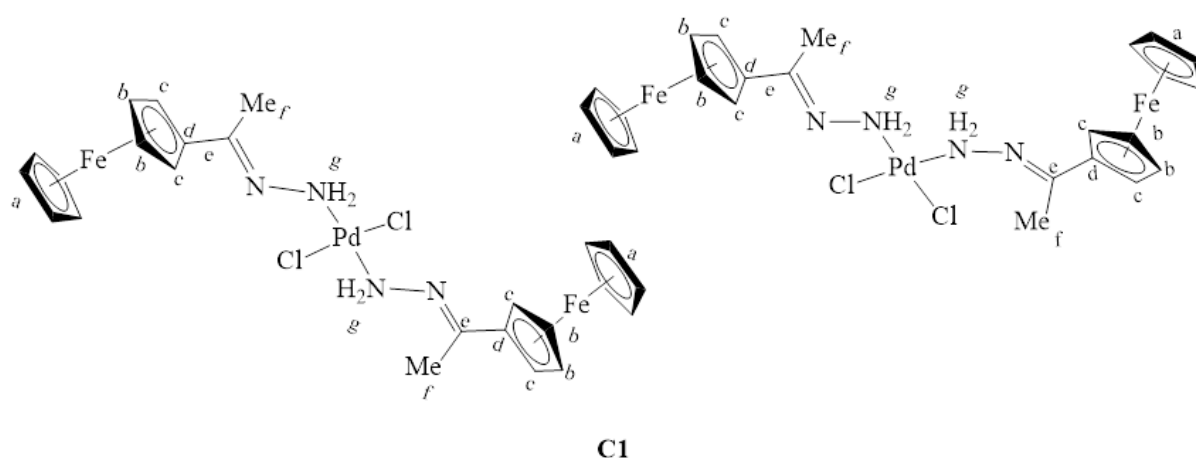

C1

Figure 27. The chemical structures of **C1** isomers.

3.3.2. Synthesis of [PdCl$_2$(**L2**)], **C2**

Bis(acetonitrile)dichloropalladium(II) (0.146 g, 0.564 mmol) was dissolved in acetonitrile (30 mL) followed by the addition of **L2** (0.240 g, 0.564 mmol) while stirring. This solution was refluxed at 85 °C for 72 h. A dark purple suspension formed, and this suspension was collected using gravity filtration and washed with warm acetonitrile (10 mL × 4). Then, the filtrate was taken, and the solvent was removed using a rotary evaporator and a purple solid resulted. The purple solid was re-dissolved in 5 mL DCM, and excess hexane was added to isolate further the desired product (**C2**, Figure 28), which was also a purple precipitate. This was achieved by collecting the purple precipitate using gravity filtration, and the purple precipitate was dried under vacuum for 8 h. Yield: 0.104 g, 31%. Melting point: decomposes without melting; onset occurs at 196 °C. FT-IR (ATR, ν_{max}/cm^{-1}): 3092 (N-H), 1563 (C=N). ^{1}H-NMR (DMSO-d_6): δ ppm = 2.17 (s, 3H, H$_f$), 4.15–4.32 (br m, 5H, H$_a$), 4.42–4.48 (br s, 2H, CH$_{Fc}$), 4.67–4.85 (br s, 2H, CH$_{Fc}$), 6.70 (br s, 1H, H$_g$), 7.29–7.71 (br m, 10H, H$_{i-j}$). ^{13}C{^{1}H}-NMR (DMSO-d_6): δ ppm = 26.6 (C$_f$), 68.9 (br m, CH$_{Fc}$), 69.2 (CH$_{Fc}$), 71.4 (CH$_{Fc}$), 78.7 (C$_d$), 127.7 (br m, C$_j$), 130.7 (br m, C$_i$), 131.5 (C$_h$), 177.6 (C$_e$). ^{31}P{^{1}H}-NMR (DMSO-d_6): δ = 105.8 ppm. Elemental Analysis (Calculated % for C$_{24}$H$_{23}$Cl$_2$FeN$_2$PPd): C 47.76, H 3.84, N 4.64. Found %: C 47.97, H 4.16, N 4.52. ESI-MS(+): m/z = 601.9893 [M]$^+$.
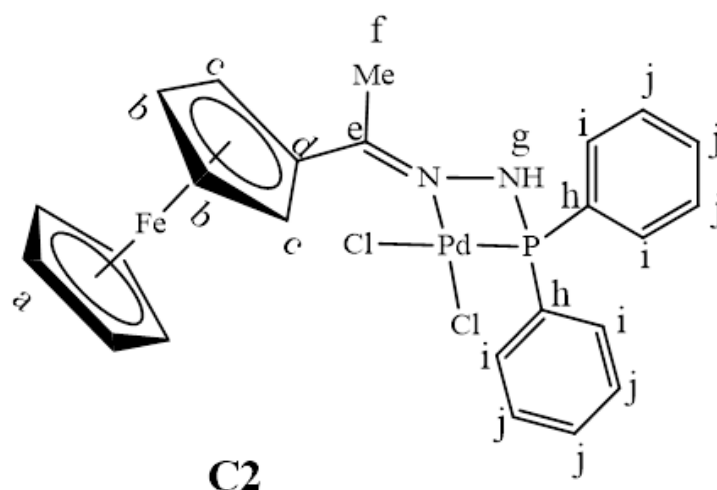
Figure 28. The chemical structure of **C2**.

3.3.3. Synthesis of [PdCl$_2$(**L3**)], **C3**

Bis(acetonitrile)dichloropalladium(II) (0.0757 g, 0.292 mmol) was added to a solution of **L3** (0.150 g, 0.292 mmol) in 30 mL of dry DCM. This solution was then stirred at room temperature for 24 h. A purple precipitate formed and was collected by gravity filtration. To obtain more of the purple solid product, the solvent was removed from the filtrate to give **C3** (Figure 29). The combined purple solid (**C3**) was dried under vacuum for 4 h. **Yield:** 0.0987 g, 49%. Melting point: decomposes without melting, onset occurs at 150 °C. FT-IR (ATR, v_{max}/cm^{-1}): 1583, 1600 (C=N). ^{1}H-NMR (DMSO-d_6): δ ppm = 2.08 (s, 3H, H$_m$), 4.30 (s, 5H, H$_q$), 4.51 (s, 2H, CH$_{Fc}$), 4.71 (s, 2H, CH$_{Fc'}$), 7.03 (br s, 1H, H$_f$), 7.53 (br m, 11H, H$_{a-c}$ and H$_g$), 7.92 (br s, 1H, H$_h$), 8.15 (br s, 1H, H$_i$), 8.29 (br s, 1H, H$_k$). ^{13}C{^{1}H}-NMR (DMSO-d_6): δ ppm = 17.0 (C$_m$), 69.2 (CH$_{Fc}$), 70.4 (CH$_{Fc}$), 70.9 (CH$_{Fc}$), 79.9 (C$_n$), 128.6–128.7 (br d, $^1J_{C-H}$ = 129.7 Hz; C$_a$, C$_b$, C$_h$), 131.9 (C$_g$), 132.9 (C$_c$), 133.5 (C$_f$), 134.1–134.3 (br m, C$_e$, C$_d$), 135.6 (C$_j$), 136.4 (C$_i$), 154.6 (C$_k$), 169.0 (C$_l$). ^{31}P{^{1}H}-NMR (DMSO-d_6): δ = 27.7 ppm. Elemental Analysis (Calculated % for C$_{31}$H$_{27}$Cl$_2$FeN$_2$PPd): C 53.83, H 3.93, N 4.05. Found %: C 54.01, H 3.87, N 3.82. ESI-MS(+): *m/z* = 655.0021 [M-Cl]$^+$.
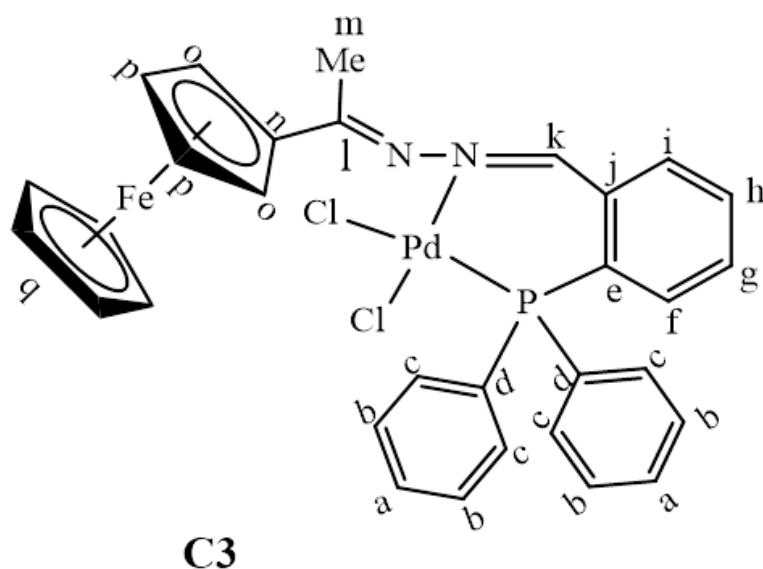

Figure 29. The chemical structure of **C3**.

3.3.4. Synthesis of [PdCl$_2$(**L4**)], **C4**

L4 (0.0673 g, 0.160 mmol) was dissolved in DCM 20 (mL) and *bis*(acetonitrile)dichloro-palladium(II) (0.0416 g, 0.160 mmol) in DCM (20 mL) was added to this stirring solution. The resulting solution was then stirred at room temperature for 48 h. A purple precipitate formed and was collected by gravity filtration. To obtain more of the purple solid product, the solvent was removed from the filtrate to give **C4** (Figure 30). The combined purple solid (**C4**) was dried under vacuum for 4 h. Yield: 0.0490, 56%. Melting point: decomposes without melting, onset occurs at 200 °C. FT-IR (ATR, ν_{max}/ cm^{-1}): 1557, 1584, 1612 (C=N). ^{1}H-NMR (DMSO-d_6): δ ppm = 2.36 (s, 3H, H$_h$), 4.29 (s, 5H, H$_l$), 4.55 (s, 2H, H$_k$), 4.75 (s, 2H, H$_j$), 7.82 (br s, 1H, H$_d$), 8.03 (br s, 2H, H$_{b,c}$), 8.33 (br s, 1H, H$_f$), 8.92 (br s, 1H, H$_a$). ^{13}C{^{1}H}-NMR (DMSO-d_6): δ ppm = 17.8 (C$_h$), 69.8 (C$_l$), 70.9 (C$_k$), 79.2 (C$_j$), 95.8 (C$_i$), 127.0 (C$_b$), 140.6 (C$_d$), 143.6 (C$_c$), 145.5 (C$_a$), 149.2 (C$_e$), 158.1 (C$_f$), 169.9 (C$_g$). Elemental Analysis (Calculated % for C$_{18}$H$_{17}$Cl$_2$FeN$_3$Pd: C 42.51, H 3.31, N 8.26. Found %: C 42.63, H 3.28, N 8.39. ESI-MS(+): m/z = 471.9414 [M-Cl]$^+$.
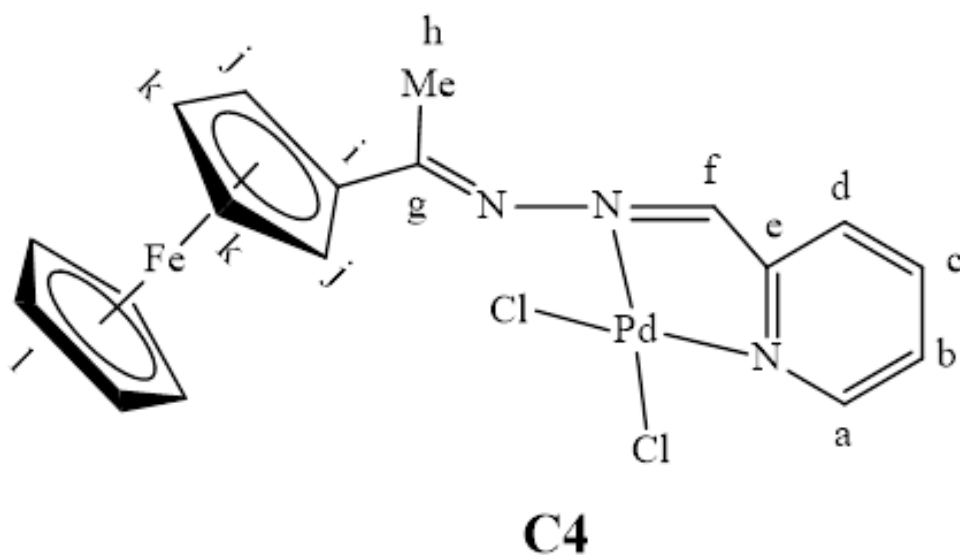

Figure 30. The chemical structure of **C4**.

3.4. General Experimental Description of Mizoroki-Heck C-C Cross-Coupling Reactions

The Mizoroki-Heck cross-coupling reaction was performed in a carousel using 24 × 150 mm quick-thread glass reaction tubes. The general approach involves charging the reaction vessel with required amounts of aryl alkene, aryl halide base, solvent and internal standard (*n*-decane). Initially, the GC was first calibrated using standard samples of all the components that are involved in the reaction vessel, thus; aryl halide, *n*-decane, solvent and *trans*-stilbene, *trans*-ethyl/methyl cinnamate, *cis*-ethyl/methyl cinnamate and *cis*-stilbene to accurately determine the retention times of these compounds. Time zero was determined by taking a sample of the reaction mixture in the reaction vessel and analyzed by GC to determine the ratios of various components. The required catalyst amount (mol%) was then added, and the reaction proceeded with a stirring rate of 600 rpm. After reaction time had elapsed, aryl halide conversion to products was calculated by analyzing retention peak areas of the aryl halide with reference to internal standard *n*-decane (See supporting information (**S**); Figures S17 and S18).

3.5. General Experimental Details for the Suzuki-Miyaura C-C Cross-Coupling Reactions

The Suzuki-Miyaura cross-coupling reactions were performed in a carousel using 24 × 150 mm quick-thread glass reaction tubes. The general procedure is similar to that given for Mizoroki-Heck Cross-coupling reactions; however, boronic acid is used herein instead of an alkene. The GC was initially calibrated using standard samples of boronic acid, toluene, *n*-decane and aryl halide to determine the retention times of these compounds accurately. Also, the reaction mixture in the reaction vessel was sampled to determine time

zero and analyzed by GC to determine the ratios of various components. The required catalyst amount (mol%) was then added, and the reaction proceeded with a stirring rate of 600 rpm. Upon the elapse of the reaction time, the aryl halide conversion to biphenyl has been calculated by analyzing retention peak areas of the aryl halide with reference to *n*-decane being the internal standard.

3.6. Computational Details on Mizoroki-Heck Cross-Coupling Reaction

Initially, all calculations were conducted using Spartan 14 Molecular Modeling program (Wavefunction, Kumasi, GH, Ghana, 2014) at the Semi-empirical PM3 level of theory. The molecular systems' geometries were first constructed using SPARTAN's graphical model builder and were also minimized interactively using the Sybyl force field. All geometries were fully optimized with some symmetry constraints where applicable on Spartan 14.

Full frequency calculations were applied on optimized geometries to verify the nature of the stationary points. The infrared spectrum output was used to characterize the equilibrium geometry by the absence of imaginary frequencies. The evaluation of transition state structures we investigated and construction of a series of constrained geometry optimizations, in which the forming-bonds and breaking-bonds were fixed at various lengths. At the same time, the remaining internal coordinates were optimized. The approximate stationary points from this procedure were fully optimized using the standard transition state optimization procedure in SPARTAN 14. An imaginary vibrational frequency was used to characterize the transition state geometries along the reaction coordinate. All the computations were performed on Dell Precision T3400 workstation computers. All calculations were then submitted to the Centre of High-Performance Computing (CHPC) using the lengau.chpc cluster for further analysis. DFT/MO6, Gaussian using 6–31G* basis set (hydrogen to argon), with quasi-relativistic effective core potentials LANL2DZ was used. All ran under vacuum at 298 K. All reported energies are relative Gibbs free energies.

3.7. General Procedure for the Isolation of Cross-Coupling Products

The crude product from Mizoroki-heck and Suzuki-Miyaura cross-coupling systems were dissolved in 100 mL of ethyl acetate and subjected to aqueous solution extraction by washing with 100 mL of water (×3). The organic layer was combined then dried using $MgSO_4$, followed by filtration and evaporation of solvent under vacuo. The residue was the re-dissolve in 2 mL DCM and further purified by passing through a column chromatography packed with silica gel and a mixture of ethyl acetate and hexane was used as an eluent of the desired product. The product were successfully isolated, the proton NMR and carbon-13 NMR have been deposited in the supplementary information section (Figures S19–S38).

3.8. Electrochemical Studies Experimental Details

Electrochemical studies conducted with use of bio-logic SP-200 potentiostat affixed to a data controller. A three-electrode system was used in the experiment with a glassy carbon electrode (GCE) as the working electrode. Finally, as also required, Ag/AgCl electrode (saturated KCl) and Pt-electrode were used as the reference and counter electrodes, respectively.

4. Summary and Conclusions

In Mizoroki-Heck coupling, all pre-catalysts **C1–C4** gave good product conversions of greater than 91% in the coupling of iodobenzene with styrene and were selective towards (*E*)-stilbene. The ferrocenylimine palladium pre-catalyst **C2** and **C3** gave moderate results for the coupling of iodobenzene with the challenging substrate α-methyl styrene. Good product conversions (>98%) were also obtained when coupling iodobenze with methyl acrylate and ethyl acrylate, which proved that all the pre-catalysts **C1–C4** have the ability to tolerate different functional groups such as esters.

The mechanistic pathways and the efficiency of pre-catalyst **C3** were investigated for the Mizoroki-Heck C-C cross-coupling reactions of iodobenzene with styrene using computational predictions by Density functional theory (DFT). This was achieved by evaluating the proposed mechanistic pathways for the catalytic steps involved in Mizoroki-Heck cross-coupling reactions. The active species, Pd^0, was generated in situ followed by the oxidative addition of iodobenzene to Pd^0. The alkene (styrene) insertion followed and showed to possibilities of insertion, which were modelled to obtain the likely insertion mode to favour stilbene over 1,1-diphenyl ethylene. Finally, the reductive elimination step and the regeneration of the active species revealed favourable energy demand and for expulsion of *E*-stilbene over *Z*-stilbene.

Moreover, ferrocenyl Pd(II) complexes **C1**, **C2** and **C4** and their corresponding ligands were subjected to cyclic voltammetry, wherein they demonstrated better stability towards redox activity relative to their corresponding ligands. This provided evidence that the coordination to palladium induces added redox stability.

In Suzuki-Miyaura coupling, bromobenzene and phenylboronic acid were used as model substrates in finding optimum reaction conditions which favoured the use of; DMF, KOH, 150 °C, and 3 h of reaction time. The pre-catalysts were active towards the coupling of bromobenzene with activated and deactivated phenylboronic acids, and also the coupling of activated and deactivated bromobenzene with phenylboronic acid. Interestingly, there was marginal difference between the use of activated and deactivated phenylboronic acids (*p*-tolylboronic acid and 4-chloroboronic acid) with bromobenzene. The more challenging activated and deactivated aryl chlorides were also coupled with phenylboronic acid using **C3** which revealed more improved activity when the activated aryl chloride was used compared to the deactivated.

Supplementary Materials: The following electronic supplementary information are available online at https://www.mdpi.com/article/10.3390/catal11070755/s1, **Figure S1**: ^{1}H NMR spectrum of ferrocenyl hydrazone **L1**, recorded in DMSO-d_6 at 25 °C, **Figure S2**: ^{31}P NMR spectrum of **L2**, recorded in CDCl$_3$ at 25 °C, **Figure S3**: ^{1}H NMR spectrum of **L3**, recorded in DMSO-d_6 at 25 °C, **Figure S4**: ^{1}P NMR spectrum of **L3**, recorded in DMSO-d_6 at 25 °C, **Figure S5**: ^{1}H NMR spectrum of **L4**, recorded in DMSO-d_6 at 25 °C, **Figure S6**: ^{1}H NMR spectrum of dichloro-bis(ferrocenyliminehydrazone)palladium(II) complex **C1**, recorded in DMSO-d_6 at 25 °C (**a**); ^{1}H NMR spectrum of **C1** after fours in room temperature, recorded in DMSO-d_6 at 25 °C (**b**), **Figure S7**: ^{31}P{^{1}H} NMR spectrum of **C2**, recorded in DMSO-d_6 at 25 °C, **Figure S8**: High resolution electrospray ionisation mass spectrum of **C3**, recorded in the positive mode, **Figure S9**: The HSQC 2D NMR of **C3** showing the region –*CHA*r*P***Ph₂**, recorded in DMSO-d_6 at 25 °C, **Figure S10**: Temperature optimization in Mizoroki-Heck cross-coupling reactions carried out using **C1**–**C4** as catalyst precursors. Reaction conditions**:** Temperature optimization. Reactions carried out in DMF (1.2 mL) with 0.66 mmol iodobenzene, 0.726 mmol of styrene, 1.32 mmol of Et$_3$N and 0.5 mol % Pd catalyst loading using *n*-decane as internal standard and the reactions were allowed to run for 4 h, **Figure S11**: Base optimization in Mizoroki-Heck cross-coupling reactions carried out using (pre)catalysts **C1**–**C4**, WB = Without Base. Reaction conditions: Reactions carried out in DMF (1.2 mL) with 0.66 mmol iodobenzene, 0.726 mmol of styrene, 1.32 mmol of base and 0.5 mol % Pd catalyst loading (**C1**–**C4**). The *n*-decane was used as internal standard and the reactions were allowed to run for 4 h at 110 °C, **Figure S12**: Time optimization in the Mizoroki-Heck cross-coupling reaction carried using (pre)catalyst **C3**, also includes effect of reaction time on TOF. Reaction conditions: Reaction time optimization using **C3**. Reactions carried out in DMF (1.2 mL) with 0.66 mmol iodobenzene, 0.726 mmol of styrene, 1.32 mmol of Et$_3$N and 0.5 mol % Pd catalyst loading using *n*-decane as internal standard and the reactions were allowed to run for 1–4 h, **Figure S13:** Optimization of catalyst loading in the Mizoroki-Heck cross-coupling reaction carried out (pre)catalyst **C3**. Reaction conditions: Catalyst loading optimization using **C3**. Reactions carried out in DMF (1.2 mL) with 0.66 mmol iodobenzene, 0.726 mmol of styrene, 1.32 mmol of Et$_3$N and 0.1–0.5 mol % Pd catalyst loading using *n*-decane as internal standard and the reactions were allowed to run for 3 h at 110 ° C, **Figure S14:** Temperature optimization in Suzuki-Miyaura cross-coupling reactions carried out using **C2** and **C4** as catalyst precursors. Reaction conditions: Reactions carried out in DMF (1.2 mL) with 0.67 mmol of bromobenzene, 1.06 mmol of phenylboronic acid, 1.33 mmol of KOH and 0.5 mol % Pd catalyst loading using *n*-decane as internal standard and

the reaction was allowed to run for 3 h at 150 °C, **Figure S15:** Solvent variation in Suzuki-Miyaura cross-coupling reactions carried out using pre-catalysts **C1–C4**. Reaction conditions: Reactions carried out in 1.2 mL (DMF/Dioxane/Toluene) with 0.67 mmol of bromobenzene, 1.06 mmol of phenylboronic acid, 1.33 mmol of KOH and 0.5 mol % Pd catalyst loading using *n*-decane as internal standard and the reaction was allowed to run for 3 hours at 150 °C (**C1–C4**), **Figure S16:** Base optimization in Suzuki-Miyaura cross-coupling reactions carried out using pre-catalysts **C1–C4**, WB = Without base. Reaction conditions: Reactions carried out in DMF (1.2 mL) with 0.67 mmol of bromobenzene, 1.06 mmol of phenylboronic acid, 1.33 mmol of (KOH/pyridine/KOH/K2CO3) and 0.5 mol % Pd catalyst loading using *n*-decane as internal standard and the reaction was allowed to run for 3 hours at 150 °C (**C1–C4**), **Figure S17**: A representation of the gas chromatogram before the Mizoroki-Heck cross-coupling reaction of iodobenzene with styrene, **Figure S18**: A representation of the gas chromatogram after 3 hours of the Mizoroki-Heck cross-coupling reaction of iodobenzene with styrene, **Figure S19**: ^{1}H NMR spectrum of **stilbene**, recorded in CDCl$_3$ at 25 °C, **Figure S20**: ^{13}C NMR spectrum of **stilbene**, recorded in CDCl$_3$ at 25 °C, **Figure S21**: ^{1}H NMR spectrum of **4-methylstilbene**, recorded in CDCl$_3$ at 25 °C, **Figure S22**: ^{13}C NMR spectrum of **4-methylstilbene**, recorded in CDCl$_3$ at 25 °C, **Figure S23**: ^{1}H NMR spectrum of **4-chlorostilbene**, recorded in CDCl$_3$ at 25 °C, **Figure S24:** ^{13}C NMR spectrum of **4-chlorostilbene**, recorded in CDCl$_3$ at 25 °C, **Figure S25:** ^{1}H NMR spectrum of **4-tert-butylstilbene**, recorded in CDCl$_3$ at 25 °C, **Figure S26**: ^{13}C NMR spectrum of **4-tert-butylstilbene**, recorded in CDCl$_3$ at 25 °C, **Figure S27**: ^{1}H NMR spectrum of **styrene ethyl acrylate**, recorded in CDCl$_3$ at 25 °C, **Figure S28**: ^{13}C NMR spectrum of **styrene ethyl acrylate**, recorded in CDCl$_3$ at 25 °C, **Figure S29**: ^{1}H NMR spectrum of **biphenyl**, recorded in CDCl$_3$ at 25 °C, **Figure S30**: ^{1}H NMR spectrum of **4-methyl biphenyl**, recorded in CDCl$_3$ at 25 °C, **Figure S31**: ^{1}H NMR spectrum of **biphenyl-4-carboxaldehyde**, recorded in CDCl$_3$ at 25 °C, **Figure S32**: ^{13}C NMR spectrum of **biphenyl-4-carboxaldehyde**, recorded in CDCl$_3$ at 25 °C, **Figure S33**: ^{1}H NMR spectrum of **2-cyanobiphenyl**, recorded in CDCl$_3$ at 25 °C, **Figure S34**: ^{13}C spectrum of **2-cyanobiphenyl**, recorded in CDCl$_3$ at 25 °C, **Figure S35**: ^{1}H NMR spectrum of **3,5-dimethoxybiphenyl**, recorded in CDCl$_3$ at 25 °C, **Figure S36**: ^{13}C NMR spectrum of **3,5-dimethoxybiphenyl**, recorded in CDCl$_3$ at 25 °C, **Figure S37**: ^{1}H NMR spectrum of **3-nitrobiphenyl**, recorded in CDCl$_3$ at 25 °C, **Figure S38**: ^{13}C NMR spectrum of **3-nitrobiphenyl**, recorded in CDCl$_3$ at 25 °C.

Author Contributions: A.C.M.: conceptualization, methodology, investigation, writing of original draft and visualization. R.T.: conceptualization, software, formal analysis. M.C.M.: Co-supervision, conceptualization, validation, Writing-review and editing. B.C.E.M.: Supervision, conceptualization, methodology, Writing—review and editing, project administration and validation. All authors have read and agreed to the published version of the manuscript.

Data Availability Statement: There is no additional data available.

Conflicts of Interest: The authors declare no conflict of interest.

References

1. Tamao, K.N.M. Cross-Coupling Reactions. In *Cross-Coupling Reaction, A Practical Guide*; Springer: New York, NY, USA, 2002; pp. 1–20.
2. Kantam, M.L.; Srinivas, P.; Yadav, J.; Likhar, P.R.; Bhargava, S. Trifunctional N,N,O-terdentate amido/pyridyl carboxylate ligated Pd(II) complexes for heck and suzuki reactions. *J. Org. Chem.* **2009**, *74*, 4882–4885. [CrossRef] [PubMed]
3. Marion, N.; Nolan, S.P. Well-Defined N-Heterocyclic Carbenes-Palladium(II) Precatalysts for Cross-Coupling Reactions. *Acc. Chem. Res.* **2008**, *41*, 1440–1449. [CrossRef] [PubMed]
4. Saito, S.; Oh-Tani, S.; Miyaura, N. Synthesis of Biaryls via a Nickel(0)-Catalyzed Cross-Coupling Reaction of Cholorarenes with Arylboronic Acids. *J. Org. Chem.* **1997**, *62*, 8024–8030. [CrossRef] [PubMed]
5. Wang, T.; Chutia, A.; Brett, D.J.L.; He, G.; Parkin, I.P.; Shearing, P.R. Environmental Science Palladium alloys used as electrocatalysts for the oxygen reduction reaction. *Energy Environ. Sci.* **2021**, *14*, 2639–2669. [CrossRef]
6. Indolese, A.F. Suzuki-type coupling of chloroarenes with arylboronic acids catalysed by nickel complexes. *Tetrahedron Lett.* **1997**, *38*, 3513–3516. [CrossRef]

7.   Farina, V. High-turnover palladium catalysts in cross-coupling and Heck chemistry: A critical overview. *Adv. Synth. Catal.* **2004**, *346*, 1553–1582. [CrossRef]

8.   Zhang, Y.; Lavigne, G.; Ce, V. Buchwald—Hartwig Amination of (Hetero)Aryl Tosylates Using a Well-Defined N-Heterocyclic Carbene/Palladium(II) Precatalyst. *J. Org. Chem.* **2015**, *80*, 7666–7673. [CrossRef]

9.   Zhang, Y.; Lavigne, G. Efficient and Versatile Buchwald–Hartwig Amination of (Hetero) aryl Chlorides Using the Pd-PEPPSI-IPr (NMe2) 2 Precatalyst in the Presence of Carbonate. *J. Org. Chem.* **2015**, 2042–2050.

10.   Tolman, C.A. Steric Effects of Phosphorus Ligands in Organometallic Chemistry and Homogeneous Catalysis. *Chem. Rev.* **1977**, *77*, 313–348. [CrossRef]

11.   Mom, S.; Beaupérin, M.; Roy, D.; Royer, S.; Amardeil, R.; Cattey, H.; Doucet, H.; Hierso, J.C. Congested ferrocenyl polyphosphanes bearing electron-donating or electron-withdrawing phosphanyl groups: Assessment of metallocene conformation from NMR spin couplings and use in palladium-catalyzed chloroarenes activation. *Inorg. Chem.* **2011**, *50*, 11592–11603. [CrossRef]

12.   Xue, L.; Lin, Z. Theoretical aspects of palladium-catalysed carbon–carbon cross-coupling reactions. *Chem. Soc. Rev.* **2010**, *39*, 1692–1705. [CrossRef]

13.   Anderson, K.W.; Ikawa, T.; Tundel, R.E.; Buchwald, S.L. The selective reaction of aryl halides with KOH: Synthesis of phenols, aromatic ethers, and benzofurans. *J. Am. Chem. Soc.* **2006**, *128*, 10694–10695. [CrossRef] [PubMed]

14.   Bruneau, A.; Roche, M.; Alami, M.; Messaoudi, S. 2-Aminobiphenyl palladacycles: The "most powerful" precatalysts in C-C and C-heteroatom cross-couplings. *ACS Catal.* **2015**, *5*, 1386–1396. [CrossRef]

15.   Kataoka, N.; Shelby, Q.; Stambuli, J.P.; Hartwig, J.F. Air stable, sterically hindered ferrocenyl dialkylphosphines for palladium-catalyzed C-C, C-N, and C-O bond-forming cross-couplings. *J. Org. Chem.* **2002**, *67*, 5553–5566. [CrossRef] [PubMed]

16.   Shu, W.; Buchwald, S.L. Use of precatalysts greatly facilitate palladium-catalyzed alkynylations in batch and continuous-flow conditions †. *Chem. Sci.* **2011**, *2*, 2321–2325. [CrossRef]

17.   Fihri, A.; Meunier, P.; Hierso, J.C. Performances of symmetrical achiral ferrocenylphosphine ligands in palladium-catalyzed cross-coupling reactions: A review of syntheses, catalytic applications and structural properties. *Coord. Chem. Rev.* **2007**, *251*, 2017–2055. [CrossRef]

18.   Feyrer, A.; Breher, F. Palladium complexes of ferrocene-based phosphine ligands as redox-switchable catalysts in Buchwald–Hartwig cross-coupling reactions. *Inorg. Chem. Front.* **2017**, *4*, 1125–1134. [CrossRef]

19.   Sollot, G.; Snead, J.; Portnoy, S.; Peterson, W., Jr.; Mertwoy, H. Aluminum chloride-catalyzed reactions of ferrocene with phosphorus(III) amides. Novel coordination of the PN system. *J. Organomet. Chem.* **1969**, *19*, 143–159. [CrossRef]

20.   Colacot, T.J. Ferrocenyl Phosphme Complexes of the Platinum Metals in Non-Chral Catalysis. *Platin. Met. Rev.* **2001**, *45*, 22–30.

21.   Ishiyama, T.; Itoh, Y.; Kitano, T.; Miyaura, N. Synthesis of arylboronates via the palladium(0)-catalyzed cross-coupling reaction of tetra(alkoxo)diborons with aryl triflates. *Tetrahedron Lett.* **1997**, *38*, 3447–3450. [CrossRef]

22.   Colacot, T.J.; Qian, H.; Cea-Olivares, R.; Hernandez-Ortega, S. Synthesis, X-ray, spectroscopic and a preliminary Suzuki coupling screening studies of a complete series of dppfMX 2 (M = Pt, Pd; X = Cl, Br, I). *J. Organomet. Chem.* **2001**, *637–639*, 691–697. [CrossRef]

23.   Vedejs, E.; Barda, D.A. Progress toward synthesis of diazonamide A. Preparation of a 3-(oxazol-5-yl)-4-trifluoromethyl-sulfonyloxyindole and its use in biaryl coupling reactions. *Org. Lett.* **2000**, *2*, 1033–1035. [CrossRef]

24.   Cousaert, N.; Toto, P.; Willand, N.; Deprez, B. Efficient, protection-free Suzuki-Miyaura synthesis of ortho-biphenyltetrazoles. *Tetrahedron Lett.* **2005**, *46*, 6529–6532. [CrossRef]

25.   Olofsson, K.; Larhed, M.; Hallberg, A. Highly Regioselective Palladium-Catalyzed Internal Arylation of Allyltrimethylsilane with Aryl Triflates synthesis, and their utility is mainly attributed to the. *J. Org. Chem.* **1998**, *3263*, 5076–5079. [CrossRef]

26.   Kang, S.; Choi, S.; Ryu, H. Palladium-Catalyzed Coupling of Organolead Compounds with Olefins. *J. Org. Chem.* **1998**, *3263*, 5748–5749. [CrossRef]

27.   Qadir, M.; Möchel, T.; Hii, K.K. Examination of ligand effects in the heck arylation reaction. *Tetrahedron* **2000**, *56*, 7975–7979. [CrossRef]

28.   Shelby, Q.; Kataoka, N.; Mann, G.; Hartwig, J. Unusual in situ ligand modification to generate a catalyst for room temperature aromatic C-O bond formation. *J. Am. Chem. Soc.* **2000**, *122*, 10718–10719. [CrossRef]

29.   Stambuli, J.P.; Stauffer, S.R.; Shaughnessy, K.H.; Hartwig, J.F. Screening of homogeneous catalysts by fluorescence resonance energy transfer. Identification of catalysts for room-temperature heck reactions. *J. Am. Chem. Soc.* **2001**, *123*, 2677–2678. [CrossRef]

30.   Teo, S.; Weng, Z.; Hor, T.S.A. 1,1′-P/O-ferrocenyl ligands in palladium-catalyzed Suzuki coupling of aryl chlorides. *Organometallics* **2006**, *25*, 1199–1205. [CrossRef]

31.   Itoh, T.; Sato, K.; Mase, T. A novel practical synthesis of C-2-arylpurines. *Adv. Synth. Catal.* **2004**, *346*, 1859–1867. [CrossRef]

32.   Itoh, T.; Mase, T. Direct synthesis of hetero-biaryl compounds containing an unprotected NH2 group via Suzuki-Miyaura reaction. *Tetrahedron Lett.* **2005**, *46*, 3573–3577. [CrossRef]

33.   Shu-Sheng, Z.; Bo, Y.; Hui-Xiang, L.; Kui, J. Facile Synthesis and Characterization of Bioactive N-[(1-Ferrocenylethylidene) amino]-N′-β-D-glycopyranosylthiourea. *Chin. J. Chem.* **2005**, *23*, 1253–1256.

34.   Vera-oyarce, C.; Aguirre, P.A.; Lagos, C.A.; Moya, S.A.; Sola, E.; Peris, G.; Bay, J.C. Methoxycarbonylation of olefins catalyzed by palladium complexes bearing P, N-donor ligands. *Dalton Trans.* **2007**, 5419–5426.

35.   Wang, P.; Liu, H.; Li, Y.; Zhao, X.; Lu, Y.; Liu, Y. Catalysis Science & Technology bifunctional ligands for sequential catalysis of. *Catal. Sci. Technol.* **2016**, *6*, 3854–3861.

36. Garrou, P.E. Ar Ring Contributions to 31P NMR Parameters of Transition-Metal-Phosphorus Chelate Complexes. *Chem. Rev.* **1981**, *81*, 229–266. [CrossRef]

37. Van Delden, R.A.; Ter Wiel, M.K.J.; Pollard, M.M.; Vicario, J.; Koumura, N.; Feringa, B.L. Unidirectional molecular motor on a gold surface. *Nature* **2005**, *437*, 1337–1340. [CrossRef]

38. Ozawa, F.; Ito, T.; Nakamura, Y.; Yamamoto, A. Mechanism of Thermal Decomposition of trans- and cis-Dialkylbis-(tertiary phosphine)palladium(II). *Bull. Chem. Soc. Jpn.* **1981**, *54*, 1868–1880. [CrossRef]

39. Oroshnik, B.Y.W.; Brown, P.K.; Habburd, R.; George, W. Rainn. *Proc. Natl. Acad. Sci. USA* **1956**, *42*, 578–580. [CrossRef] [PubMed]

40. Pollard, M.M.; Meetsma, A.; Feringa, B.L. A redesign of light-driven rotary molecular motors. *Org. Biomol. Chem.* **2008**, *6*, 507–512. [CrossRef]

41. Makhubela, B.C.E.; Jardine, A.; Smith, G.S. Pd nanosized particles supported on chitosan and 6-deoxy-6-amino chitosan as recyclable catalysts for Suzuki-Miyaura and Heck cross-coupling reactions. *Appl. Catal. A Gen.* **2011**, *393*, 231–241. [CrossRef]

42. Elgrishi, N.; Rountree, K.J.; McCarthy, B.D.; Rountree, E.S.; Eisenhart, T.T.; Dempsey, J.L. A Practical Beginner's Guide to Cyclic Voltammetry. *J. Chem. Educ.* **2018**, *95*, 197–206. [CrossRef]

43. Mabbott, G.A. An introduction to cyclic voltammetry. *J. Chem. Educ.* **1983**, *60*, 697–702. [CrossRef]

44. Powers, M.J.; Meyer, T.J. Medium and Distance Effects in Optical and Thermal Electron Transfer. *J. Am. Chem. Soc.* **1980**, *102*, 1289–1297. [CrossRef]

45. Dagdevren, M.; Yilmaz, I.; Yucel, B.; Emirik, M. A Novel Ferrocenyl Naphthoquinone Fused Crown Ether as a Multisensor for Water Determination in Acetonitrile and Selective Cation Binding. *J. Phys. Chem. B* **2015**, *119*, 12464–12479. [CrossRef] [PubMed]

46. Shahsavari, H.R.; Fereidoonnezhad, M.; Niazi, M.; Mosavi, S.T.; Habib Kazemi, S.; Kia, R.; Shirkhan, S.; Abdollahi Aghdam, S.; Raithby, P.R. Cyclometalated platinum(ii) complexes of 2,2′-bipyridine N-oxide containing a 1,1′-bis(diphenylphosphino)ferrocene ligand: Structural, computational and electrochemical studies. *Dalton Trans.* **2017**, *46*, 2013–2022. [CrossRef]

47. Mitoraj, M.P.; Michalak, A. σ-Donor and π-Acceptor Properties of Phosphorus Ligands: An Insight from the Natural Orbitals for Chemical Valence. *Inorg. Chem.* **2010**, *49*, 578–582. [CrossRef]

48. Gagne, R.R.; Koval, C.A.; Lisensky, G.C. Ferrocene as an Internal Standard for Electrochemical Measurements. *Inorg. Chem.* **1980**, *19*, 2854–2855. [CrossRef]

49. Rapakousiou, A.; Deraedt, C.; Irigoyen, J.; Wang, Y.; Pinaud, N.; Salmon, L.; Ruiz, J.; Moya, S.; Astruc, D. Synthesis and redox activity of "clicked" triazolylbiferrocenyl polymers, network encapsulation of gold and silver nanoparticles and anion sensing. *Inorg. Chem.* **2015**, *54*, 2284–2299. [CrossRef] [PubMed]

50. Berben, L.A.; Faia, M.C.; Crawford, N.R.M.; Long, J.R. Angle-dependent electronic effects in 4,4′-bipyridine-bridged Ru 3 triangle and Ru4 square complexes. *Inorg. Chem.* **2006**, *45*, 6378–6386. [CrossRef] [PubMed]

51. Toma, S.H.; Uemi, M.; Nikolaou, S.; Tomazela, D.M.; Eberlin, M.N.; Toma, H.E. {trans-1,4=bis[(4-pyridyl)ethenyl]benzene}(2,2′-bipyridine) rutherium(II) complexes and their supramolecular assemblies with β-cyclodextrin. *Inorg. Chem.* **2004**, *43*, 3521–3527. [CrossRef]

52. D'Alessandro, D.M.; Keene, F.R. Intervalence charge transfer (IVCT) in trinuclear and tetranuclear complexes of iron, ruthenium, and osmium. *Chem. Rev.* **2006**, *106*, 2270–2298. [CrossRef] [PubMed]

53. Argazzi, R.; Bertolasi, E.; Chiorboli, C.; Bignozzi, C.A.; Itokazu, M.K.; Murakami Iha, N.Y. Intramolecular energy transfer processes in binuclear Re-Os complexes. *Inorg. Chem.* **2001**, *40*, 6885–6891. [CrossRef] [PubMed]

54. Lash, T.D.; Colby, D.A.; Graham, S.R.; Ferrence, G.M.; Szczepura, L.F. Organometallic Chemistry of Azuliporphyrins: Synthesis, Spectroscopy, Electrochemistry, and Structural Characterization of Nickel(II), Palladium(II), and Platinum(II) Complexes of Azuliporphyrins. *Inorg. Chem.* **2003**, *42*, 7326–7338. [CrossRef]

55. van Asselt, R.; Elsevier, C.J.; Amatore, C.; Jutand, A. Divalent Palladium and Platinum Complexes Containing Rigid Bidentate Nitrogen Ligands and Electrochemistry of the Palladium Complexes 1. *Organometallics* **1997**, *16*, 317–328. [CrossRef]

56. Leonhardt, S.E.S.; Stolle, A.; Ondruschka, B.; Cravotto, G.; De Leo, C.; Jandt, K.D.; Keller, T.F. Chitosan as a support for heterogeneous Pd catalysts in liquid phase catalysis. *Appl. Catal. A Gen.* **2010**, *379*, 30–37. [CrossRef]

57. Buchwalter, P.; Rosé, J.; Braunstein, P. Multimetallic catalysis based on heterometallic complexes and clusters. *Chem. Rev.* **2015**, *115*, 28–126. [CrossRef]

58. Hierso, J.C.; Fihri, A.; Amardeil, R.; Meunier, P.; Doucet, H.; Santelli, M. Use of a bulky phosphine of weak σ-donicity with palladium as a versatile and highly-active catalytic system: Allylation and arylation coupling reactions at 10-1-10-4mol% catalyst loadings of ferrocenyl bis(difurylphosphine)/Pd. *Tetrahedron* **2005**, *61*, 9759–9766. [CrossRef]

59. Wu, X.F.; Anbarasan, P.; Neumann, H.; Beller, M. From noble metal to Nobel Prize: Palladium-catalyzed coupling reactions as key methods in organic synthesis. *Angew. Chem. Int. Ed.* **2010**, *49*, 9047–9050. [CrossRef]

60. Littke, A.F.; Fu, G.C. Palladium-catalyzed coupling reactions of aryl chlorides. *Angew. Chem. Int. Ed. Engl.* **2002**, *41*, 4176–4211. [CrossRef]

61. Hierso, J.C.; Fihri, A.; Amardeil, R.; Meunier, P.; Doucet, H.; Santelli, M.; Donnadieu, B. A palladium-ferrocenyl tetraphosphine system as catalyst for suzuki cross-coupling and heck vinylation of aryl halides: Dynamic behavior of the palladium/phosphine species. *Organometallics* **2003**, *22*, 4490–4499. [CrossRef]

62. Collman, J.; Hedegus, S.; Finke, R.G. *Principles and Applications of Organotransition Metal Chemistry*; University Science Books: Sausalito, CA, USA, 1987; p. 103. Available online: https://onlinelibrary.wiley.com/doi/abs/10.1002/anie.198809841 (accessed on 10 June 2021).

63. Shaughnessy, K.H. Beyond TPPTS: New approaches to the development of efficient palladium-catalyzed aqueous-phase cross-coupling reactions. *Eur. J. Org. Chem.* **2006**, 1827–1835. [CrossRef]

64. Matsinha, L.C.; Mao, J.; Mapolie, S.F.; Smith, G.S. Water-Soluble Palladium(II) Sulfonated Thiosemicarbazone Complexes: Facile Synthesis and Preliminary Catalytic Studies in the Suzuki-Miyaura Cross-Coupling Reaction in Water. *Eur. J. Inorg. Chem.* **2015**, *2015*, 4088–4094. [CrossRef]

65. Siangwata, S.; Baartzes, N.; Makhubela, B.C.E.; Smith, G.S. Synthesis, characterisation and reactivity of water-soluble ferrocenylimine-Rh(I) complexes as aqueous-biphasic hydroformylation catalyst precursors. *J. Organomet. Chem.* **2015**, *796*, 26–32. [CrossRef]

66. Widegren, J.A.; Bennett, M.A.; Finke, R.G. Is it homogeneous or heterogeneous catalysis? Identification of bulk ruthenium metal as the true catalyst in benzene hydrogenations starting with the monometallic precursor, Ru(II)(η6-C6Me 6)(OAc)2, plus kinetic characterization of the heterogeneous nucle. *J. Am. Chem. Soc.* **2003**, *125*, 10301–10310. [CrossRef]

67. Atkins, P.; Overton, T.; Rourke, J.; Weller, M.; Amstrong, F. Shriver and Atkins. In *Shriver and Atkins' Inorganic Chemistry*, 5th ed; Oxford University Press: Oxford, UK, 2009; p. 514.

68. Fitton, P.; Johnson, M.P.; McKeon, J.E. Oxidative additions to palladium(0). *Chem. Commun.* **1968**, 6–7. [CrossRef]

69. Senn, H.M.; Ziegler, T. Oxidative addition of aryl halides to palladium(0) complexes: A density-functional study including solvation. *Organometallics* **2004**, *23*, 2980–2988. [CrossRef]

70. Vyskočil, Š.; Smrcina, M.; Hanuš, V.; Polášek, M.; Kočovský, P. Derivatives of 2-Amino-2′-diphenylphosphino-1,1′-binaphthyl (MAP) and Their Application in Asymmetric Palladium(0)-Catalyzed Allylic Substitution. *J. Org. Chem.* **1998**, *63*, 7738–7748. [CrossRef]

71. García-Melchor, M.; Braga, A.A.C.; Lledós, A.; Ujaque, G.; Maseras, F. Computational perspective on Pd-catalyzed C-C cross-coupling reaction mechanisms. *Acc. Chem. Res.* **2013**, *46*, 2626–2634. [CrossRef] [PubMed]

72. Clayden, J.; Greeves, N.; Warren, S.; Wothers, P. The S_N1 and S_N2 mechanisms for nucleophilic substitution. In *Organic Chemistry*; Oxford University Press Inc.: New York, NY, USA, 2001; pp. 411–414.

73. van Leeuwen, P.W.N.M.; Kamer, P.C.J.; Reek, J.N.H. The bite angle makes the catalyst. *Pure Appl. Chem.* **1999**, *71*, 1443–1452. [CrossRef]

74. Chen, L.; Ren, P.; Carrow, B.P. Tri(1-adamantyl)phosphine: Expanding the Boundary of Electron- Releasing Character Available to Organophosphorus Compounds. *J. Am. Chem. Soc.* **2016**, *138*, 1–4. [CrossRef] [PubMed]

75. Clayden, J.; Greeves, N.; Warren, S.; Wothers, P. Electrophilic aromatic substitution. In *Organic Chemistry*; Oxford University Press Inc.: New York, NY, USA, 2001; pp. 556–571.

76. Kashin, A.S.; Ananikov, V.P. Catalytic C–C and C–Heteroatom Bond Formation Reactions: In Situ Generated or Preformed Catalysts? Complicated Mechanistic Picture Behind Well-Known Experimental Procedures. *J. Org. Chem.* **2013**, *78*, 11117–111125. [CrossRef] [PubMed]

77. Anderson, G.K.; Lin, M.; Sen, A.; Gretz, E. Bis(Benzonitrile)Dichloro Complexes of Palladium and Platinum. In *Inorganic Syntheses*; John Wiley & Sons, Inc.: Hoboken, NJ, USA, 2007; pp. 60–63.